Arctic mercury cycling

Ashu Dastoor, Hélène Angot, Johannes Bieser, Jesper Christensen, Thomas Douglas, Lars-Eric Heimbürger-Boavida, Martin Jiskra, Robert Mason, David Mclagan, Daniel Obrist, et al.

Arctic mercury cycling

Ashu Dastoor[1*], Hélène Angot[2], Johannes Bieser[3], Jesper H. Christensen[4], Thomas A. Douglas[5], Lars-Eric Heimbürger-Boavida[6], Martin Jiskra[7], Robert P. Mason[8], David S. McLagan[9], Daniel Obrist[10], Peter M. Outridge[11], Mariia V. Petrova[6], Andrei Ryjkov[1], Kyra A. St. Pierre[12], Amina T. Schartup[13], Anne L. Soerensen[14], Kenjiro Toyota[15], Oleg Travnikov[16], Simon J. Wilson[17], Christian Zdanowicz[18]

*Corresponding author: ashu.dastoor@ec.gc.ca

1. Air Quality Research Division, Environment and Climate Change Canada, Dorval, Quebec, Canada
2. Extreme Environments Research Laboratory, École Polytechnique Fédérale de Lausanne (EPFL) Valais Wallis, Sion, Switzerland
3. Institute of Coastal Research, Helmholtz-Zentrum hereon, Geesthacht, Germany
4. Department of Environmental Science, Aarhus University, Roskilde, Denmark
5. U.S. Army Cold Regions Research & Engineering Laboratory, Fort Wainwright, United States
6. Aix Marseille Université, CNRS/INSU, Université de Toulon, IRD, Mediterranean Institute of Oceanography, Marseille, France
7. Environmental Geosciences, University of Basel, Basel, Switzerland
8. Department of Marine Sciences, University of Connecticut, Connecticut, United States
9. Institute for Geoecology, Technical University of Braunschweig, Braunschweig, Germany & Department of Physical and Environmental Sciences, University of Toronto Scarborough, Toronto, Canada
10. Department of Environmental, Earth and Atmospheric Sciences, University of Massachusetts, Lowell, Massachusetts, USA
11. Geological Survey of Canada, Natural Resources Canada, Ottawa, Ontario, Canada
12. Institute for the Oceans and Fisheries, University of British Columbia, Vancouver, British Columbia, Canada
13. Scripps Institution of Oceanography, University of California San Diego, La Jolla, California, USA
14. Department of Environmental Research and Monitoring, Swedish Museum of Natural History, Stockholm, Sweden
15. Air Quality Research Division, Environment and Climate Change Canada, Toronto, Ontario, Canada
16. Meteorological Synthesizing Centre-East, EMEP, Moscow, Russia
17. Arctic Monitoring and Assessment Programme Secretariat, Tromsø, Norway
18. Department of Earth Sciences, Uppsala University, Uppsala, Sweden

Abstract| Mercury (Hg) levels in Arctic ecosystems, which rose markedly due to global anthropogenic Hg emissions since industrialization, are now being altered as the region warms, with as-yet uncertain ecological consequences. This Review presents a comprehensive assessment of the present-day total Hg mass balance (fluxes and budgets) in the Arctic from a synthesis of published research and atmospheric multi-model simulations, and identifies key future research needs. Arctic atmospheric Hg is primarily emitted outside the region (>98%), and about two-thirds of transported Hg is deposited to terrestrial

ecosystems, where it predominantly accumulates in soils via vegetation uptake. Rivers and coastal erosion annually transfer about equal amounts of terrestrial Hg (primarily from above 60° N) to the Arctic Ocean, in approximate balance with modeled net terrestrial Hg deposition in the region, though air-land Hg exchange estimates need further refinement. The revised Arctic Ocean Hg mass balance suggests net atmospheric Hg deposition to the ocean and that Hg burial in inner-shelf sediments is underestimated (up to >100%) and atmosphere-seawater-sediment Hg exchanges are poorly constrained. Specific terrestrial Hg mobilization pathways from the cryosphere (permafrost, ice, snow, and glaciers) remain largely uncertain, and need addressing to anticipate present and future climate impacts on downstream Arctic ecosystems.

Key points

1. Arctic terrestrial mercury (Hg) emissions from anthropogenic activities (14 Mg y^{-1}; <1% of global share), wildfires (8.8±6.4 Mg y^{-1}), and soil/vegetation re-volatilization (24(7-59) Mg y^{-1}) are low compared to deposition (118±20 Mg y^{-1}). Primarily driven by springtime photochemistry, Arctic Ocean Hg deposition (65±20 Mg y^{-1}) exceeds evasion (32(23-45) Mg y^{-1}), which peaks when snow/ice melt and sea ice retreats.

2. Large pools of Hg (~597,000 Mg, 0-3 m depth) have accumulated in permafrost soils, predominantly from vegetation uptake of atmospheric gaseous elemental Hg over millennia. Coastal erosion mobilizes an estimated 39(18-52) Mg y^{-1} of soil-bound Hg into the Arctic Ocean.

3. Pan-Arctic rivers export 41±4 Mg y^{-1} of dissolved and particulate Hg (~50% each) to the Arctic Ocean predominantly during the spring freshet, likely derived from seasonal snowpacks (≤ 50%) and active-layer surface soils (≥ 50%) of the watershed portion north of 60^0 N, but specific mobilization pathways are unclear.

4. Revised Arctic Ocean Hg budget (~1870 Mg) is lower than previous estimates (2847-7920 Mg), and implies higher sensitivity to changes in climate and emissions. Shelf region particulate Hg settling (122±55 Mg y^{-1}) from surface waters is the largest Hg removal mechanism in the ocean, but its annual observations are currently lacking.

5. Combined observation and modeling estimates suggest a balance of Hg mass fluxes in and out of Arctic soils, but air-terrestrial Hg exchange fluxes need further improvement. The revised Arctic Ocean Hg mass balance suggests that Hg burial in shelf sediments (42±31 Mg y^{-1}) is underestimated by up to 52.2±43.5 Mg y^{-1}.

6. Permafrost thaw leads to high concentrations of soil-derived Hg in some streams (up to 1270 ng L^{-1}), but its future impact is presently uncertain. Melt releases ~0.4 Mg y^{-1} of deposited Hg stored in Arctic glaciers (2,415 Mg), which is dwarfed by ~40 Mg y^{-1} of geogenic particulate Hg exported by glacial rivers into adjacent seas.

Introduction

Mercury (Hg) is a neurotoxic pollutant emitted by both natural and anthropogenic sources, and dispersed globally via atmospheric transport, ocean currents, and rivers. Observations over the past 40 years show that Hg concentrations in Arctic marine mammals and seabirds are elevated compared to lower latitudes [1,2]. As a result, Arctic Peoples, who harvest and consume these animals in their traditional diets, are disproportionately exposed to Hg [3,4].

Local anthropogenic Hg emissions are negligible in the Arctic, and Hg inputs to Arctic ecosystems are thus largely driven by global Hg emissions[1,5]. The existing reservoirs of Hg in Arctic air, soil, snow, ice and water are closely interlinked[6,7](Box 1). Chemical transformations between key Hg species (gaseous and dissolved elemental Hg (Hg(0)), oxidized divalent Hg (Hg(II)) and methylmercury (MeHg)), drive continuous exchanges of these species between reservoirs, influenced by sunlight, organic matter, biological activity, and other key parameters and processes[8-10]. Climate warming, which is magnified in polar regions[11,12], is anticipated to continue enhancing Hg mobilization due to higher surface temperatures, intensified wildfires[13], permafrost thaw[14,15], glacier[16-18] and sea ice melt[19], and increased river discharge.

The Arctic is a remote region with a paucity of historical Hg observations. However, in recent decades major research initiatives have expanded the spatio-temporal scope of measurements[19-24], used new techniques such as stable Hg isotopes[25-29], elucidated redox chemistry[30,31] and undertaken process-based modeling[6,32-35]. This has greatly improved our understanding of Hg fluxes and processes in the Arctic, underpinning the revision of its mass balance described here. A few global Hg reviews or assessments of different topics[36-38] have included some Arctic Hg data in their syntheses. This review represents the first comprehensive re-examination of the Arctic Hg cycle and mass balance since 2011[1].

In this Review, an updated understanding of the total Hg mass balance in the Arctic is developed from literature synthesis and modeling conducted for the Arctic Monitoring and Assessment Programme (AMAP) 2021 Hg Assessment. Other parts of the AMAP 2021 Assessment concerned Hg methylation/demethylation, and Hg concentrations and trends in biota, which are not covered here. Arctic mercury fluxes (emissions and depositions, oceanic inflow/outflow, particle settling and sediment burial, river export, coastal erosion, sea ice export) and reservoir mass budgets (atmosphere, permafrost soils, seasonal snowpacks, glaciers, sea ice, and ocean) are developed for the land area north of 60^0 N and the Arctic Ocean (AO) - defined as the central basin and the Barents, Kara, Laptev, East Siberian, Chukchi and Beaufort Seas (Fig. S1). The significance of these estimated fluxes to Hg cycling in Arctic ecosystems is examined, and future research areas are prioritized based on current uncertainties. This

Review benchmarks contemporary total Hg pathways and levels in the Arctic, and supports the effectiveness evaluation objective of the *Minamata Convention on Mercury*.

Atmospheric mercury

Each year 6,000-9,000 Mg of Hg is emitted to the atmosphere[44] through anthropogenic activities (2,000–3,000 Mg) [39,40], biomass burning (400-700 Mg)[41-43], and geogenic degassing and legacy emissions from land (1,000–1,600 Mg)[37] and oceans (2,700–3,400 Mg)[37], mainly as Hg(0) (0.5-1 year lifetime) with some as Hg(II) (1-2 weeks lifetime). Atmospheric Hg is transported to the Arctic from global sources, driven by synoptic-scale pressure systems. Hg transport is enhanced from northern Eurasian sources in winter, influenced by the Arctic polar dome, and from mid-latitude Asian and North American sources in spring, facilitated by convective lifting[44-48].

Changes in air circulation patterns due to warmer temperatures and lower sea ice concentrations with a warming climate[49,50] are impacting contaminant transport to and within the Arctic[51] including Hg transport and deposition[5,35,52]. Following sections describe atmospheric Hg emission sources, transport and deposition pathways, and concentrations and deposition patterns in the Arctic.

Anthropogenic and wildfire emissions

Less than 1% of estimated global annual anthropogenic Hg emissions to air (~14 Mg, 2015) are emitted from sources within the Arctic[39,53]. Main sources of Hg emissions in the Arctic are point sources in northern Russia, including non-ferrous metal smelters and coal-fired power plants[53]. Other sources of anthropogenic Hg emissions in the Arctic include mining, oil and gas activities, and uncontrolled disposal of waste that might contain Hg-added products. The methodological assumptions made in estimating anthropogenic Hg emissions and their geospatial distribution, especially from non-point sources in areas of sparse population, mean that they are subject to large uncertainty.

In the Arctic, Hg emissions from open biomass burning are primarily related to natural (wildfire) sources, predominantly boreal forest fires. Hg in biomass is almost exclusively derived from atmospheric deposition and is released through the combustion of living and ground litter, and soil heating during wildfires[54,55]. Annual Hg emissions estimates from open biomass burning vary widely, ranging from ~20 Mg[54,56] to 200 Mg[42], with large uncertainties, particularly for boreal forest fires. The uncertainty is associated with high interannual variability in the burned area of boreal forests and use of non-biome specific Hg emissions ratios (enhanced concentration ratio of Hg and a co-pollutant) or emissions factors (Hg mass emitted per area burned) with assumed carbon species emission enhancements[41-43]. Further, these empirical emission ratios or factors are often measured at sites distant from fire sources, which

likely lead to overestimation of Hg emissions due to the shorter atmospheric lifetime of carbon monoxide (CO) and variability in CO emissions based on vegetation-type and fire intensity[56]. Following the empirical emission factor-based method (EEM3)[56], an improved mean atmospheric Hg emission from Arctic fires (>60°N) is estimated as 8.8±6.4 Mg y^{-1} for the period 2001-2019. This emission estimate uses the mean emission factor from two near source boreal forest aircraft studies[54,56], mean burned area based on three separate algorithms[57-59], mean total fuel consumption (including soil carbon releases) of Canadian Arctic biomes (2.31±0.81 kg m^{-2})[60], complete (100±5%)[54,56] release of Hg during fires, and atmospheric Hg fractions of 96.2% elemental and 3.8% particulate.

The current push for natural resource development in the Arctic (oil and gas exploration, mining) could lead to greater anthropogenic Hg releases within the region. Additionally, human development in the Arctic is projected to increase due to climate change, raising the potential for increasing anthropogenic Hg sources. Boreal peatlands are estimated to contain ten times greater Hg stocks than in boreal forests due to a thicker organic layer[61], and likely release more Hg during fires. The Hg speciation of peat fire emissions might differ due to more dominant smoldering (vs. flaming) combustion[62]. Global fire emissions databases indicate a larger increasing trend in wildfires (frequency, intensity, and burning season length) north of 60^0 between 2005-2018 than 50-60^0 N, partly attributed to human activities[63-66].

Air-surface Hg exchange

Hg exchange between the Earth's surface and the atmosphere occurs via several pathways[67]: Hg(0) exchange with vegetation, soils, snow, ice and waters; and atmospheric oxidation of Hg(0) and subsequent wet and dry Hg(II) deposition in gaseous or particulate phase. Vegetation uptake of atmospheric Hg(0) is the dominant deposition pathway in vegetated Arctic ecosystems (~70% of total deposition), when compared to the Hg(II) deposition[37,68]. Hg oxidation and deposition processes intensify during springtime (known as atmospheric mercury depletion events (AMDEs)) in coastal and marine Arctic environments[69], facilitated by excessive photochemical release of gaseous bromine to air from snowpacks on sea ice, wind-blown snow particles and sea-salt aerosols[70-73]. However, 40-90% of Hg deposited during AMDEs is photo-reduced and reemitted[66]. Hg(0) evasion rates are low in the interior tundra in all seasons[68,74] and high from marine waters during spring/summer sea ice retreat[19].

For this Review, the contemporary atmospheric Hg cycle (year 2015) was simulated (Fig. 1) using an ensemble of Hg models[33,75] (GLEMOS[76], GEOS-Chem[34,77], GEM-MACH-Hg[52,78-80], DEHM [81,82]; see details of the models in the Supplementary Information Text S1, Table S1). Arctic atmospheric mercury concentrations are shaped by transport patterns from lower latitudes and deposition processes in the

Arctic[1]. Air Hg(0) concentrations in the Arctic (1.4 ng m^{-3}, modeled and measured[83-85] domain annual average) are characterized by a latitudinal gradient with concentrations greater than 1.4 ng m^{-3} occurring across most of the terrestrial Arctic and concentrations less than 1.4 ng m^{-3} over the Canadian Arctic Archipelago (CAA), Greenland and the AO (Fig. 1a). In the Arctic, the strongest Hg(0) seasonal cycle is observed in coastal and marine regions (1.1-1.6 ng m^{-3}, monthly mean range)[33]. Minimum Hg(0) concentrations, driven by AMDEs, are observed in spring, and maximum concentrations occur in summer that are attributed to snow and sea ice melt and oceanic Hg re-emissions[33,78,86]. Total oxidized Hg concentrations at high Arctic coastal sites are an order of magnitude higher in springtime (>150 pg m^{-3}, 10 years mean observed at Alert, Canada) than the remainder of the year (<25 pg m^{-3}, Alert)[87]. Arctic atmospheric Hg levels are less dynamic in fall and winter, and primarily reflect northern hemispheric background Hg[86]. The models accurately simulate the seasonal cycle of atmospheric mercury species[33], but underestimate the amplitude of the seasonal variation due to a lack of real-time mechanistic modeling of the production of bromine species and sea ice dynamics[78,88].

The Arctic is characterized by low wet deposition fluxes (<5 μg m^{-2} y^{-1}, modeled; <4 μg m^{-2} y^{-1}, observed[76,89]), especially in arid areas of Greenland, the CAA, and Siberia, compared to lower latitudes (up to 30 μg m^{-2} y^{-1})[90-92] (Fig. 1b). While precipitation Hg concentrations in the Arctic are low most of the year, springtime snowfall Hg concentrations can be anomalously high during AMDEs, especially in coastal and marine locations (for example, median total Hg snowfall concentrations of 79-388 ng L^{-1} in March, Utqiagvik, Alaska)[93]. Models overestimate Hg wet deposition flux by up to 100% compared to observations[8-10,94]. However, measured Hg wet deposition fluxes are likely significantly underestimated in polar regions due to measurement challenges. Wet deposition collectors have lower collection efficiencies for snow than the recommended precipitation gauges (by ~30%)[95]. However, precipitation gauges also underestimate snowfall amounts by 20-50% in windy environments[96-98], and are subject to the uncertainties of measuring trace precipitation prevalent in the Arctic[99,100].

Model ensemble annual average total Hg deposition flux rates in the Arctic are 6.8±1.2 μg m^{-2} y^{-1}(5.2±1.2 μg m^{-2} y^{-1}, north of 66.5^0 N) over land and 7.4±1.6 μg m^{-2} y^{-1} over the AO with about half of seasonal contributions occurring in summer over land and in spring over ocean (Table S2; Fig. 1c). Highest modeled Hg deposition rates (up to 20 μg m^{-2} y^{-1}) occur in the regions characterized by: presence of local Hg emissions (Fennoscandia); efficient trans-Pacific transport (northwestern North America); high net primary productivity (boreal forests); and higher precipitation amounts (ocean around Greenland, and coastal northwestern Europe and North America) (Fig. 1c). Over land, Hg deposition rates decline from south to north and west to east in Eurasia and North America, driven by proximity to Hg emission

sources. Compared to the measured[68] Hg deposition flux of 9.2 μg m^{-2} y^{-1} at a tundra (Alaska) site, the model ensemble-estimated deposition flux is 7.2±2.2 μg m^{-2} y^{-1} (~22% lower). GEM-MACH-Hg model-simulated median dry deposition Hg flux in boreal forests (8.3 (3.5–15.1) μg m^{-2} y^{-1})[37] is consistent with the litterfall-based estimate (8.6 (1.3–19.8 μg m^{-2} y^{-1})[97], but underestimated in Arctic tundra (4.2 (1.1–8.8)[44] μg m^{-2} y^{-1}, model; 6.0 (1.4–17)[101] μg m^{-2} y^{-1}, litterfall-based). Modeled deposition compares well with lake sediment-inferred average Hg deposition rates in the Canadian high Arctic[102,103] and sub-Arctic[102,104,105] of 3.5 μg m^{-2} y^{-1} (~ 3.6 μg m^{-2} y^{-1} (0.5–5 μg m^{-2} y^{-1}), modeled) and 7.5-10.0 μg m^{-2} y^{-1} (~7.65 μg m^{-2} y^{-1} (5–10 μg m^{-2} y^{-1}), modeled), respectively. Model ensemble wintertime (September-May) deposition is also consistent with observation-based [29,106,107] deposition at the three high Arctic sites (~2-4 μg m^{-2}).

Model ensemble estimates Arctic atmospheric total Hg burden of 330 Mg (290-360 Mg, seasonal variance), and total deposition of 243±41 Mg y^{-1} (~51% deposited to the ocean) north of 60°N. Model ensemble total deposition estimate of 133±31 Mg y^{-1} north 66°N in 2015 is in line with the literature range of 110-131 Mg y^{-1} [76,78,81]. Modeling estimates of Hg(0) evasion flux from soils and vegetation is 24 (7-59) Mg y^{-1} (model ensemble), and from the AO are 23.3 (GEM-MACH-Hg) and 45.0 Mg y^{-1} (GEOS-Chem). Air-sea Hg exchange fluxes are highly dynamic in spring and summer as a result of AMDEs[108], snow/sea ice melt and river discharge[34-36,80], but open ocean measurements representing all seasons are lacking to confirm model estimated marine Hg fluxes[19,109,110].

Long-term Hg observations at high Arctic sites show seasonally variable and overall neutral (Ny-Ålesund, Svalbard)[111] to decreasing (≤ 1.0% per year, Alert[83] and Villum Research Station, Greenland[82]) air concentrations of Hg(0), and increasing springtime Hg(II) concentrations (9–17% per year, Alert[83]). Climate warming led changes in AMDEs-related oxidation chemistry[83], air-surface Hg exchanges[5,52] and increasing precipitation[52] with consequences to Hg deposition in the Arctic are suggested to be responsible for the changing atmospheric mercury cycling. Vegetation Hg deposition is projected to increase with increasing vegetation cover and density[32,112], but Hg evasion from soils is projected to increase in response to accelerating wildfires and permafrost thaw-led microbial reduction and release of stored Hg in soils[15].

Current and projected future Arctic warming trends[113] towards an increase in thinner first year sea ice, more open sea ice leads, a longer open water season, and increased ice dynamics, might favor conditions that stimulate AMDE-related Hg deposition by enhancing reactive halogen sources. A 22-year (1996-2017) trend analysis of Arctic atmospheric bromine monoxide (BrO) satellite measurements[114] found moderate spatiotemporal relationship ($r = 0.32$, $p < 0.05$) between springtime BrO concentrations and the

first-year sea ice extent in the AO, both having increased over this period. Higher temperature is suggested to decrease the Hg oxidation via Br-initiated reactions owing to the thermal dissociation of HgBr[115,116], but the transformation of HgBr to BrHgO via ozone reaction likely dominates over the thermal dissociation[117] resulting in weaker temperature dependence of Hg oxidation. Convective mixing over more prevalent open leads can increase Hg(0) supply in near-surface air to be oxidized and deposited to surrounding snowpacks [118,119].

Terrestrial mercury

The terrestrial system plays a dual role in Arctic Hg cycling as a sink of atmospheric Hg and as a source of Hg to surface waters[7]. The importance of terrestrial Hg exports to the AO is supported by soil-like Hg stable isotope signatures in marine sediments and biota[120,121]. Hg lifetime in Arctic terrestrial reservoirs ranges between ~10^3 (soils), 10^2-10^3(glaciers) and 1 (snowpack) year, which might be reduced in future due to Arctic warming led large perturbations of the terrestrial system[38]. In the following, we discuss Hg distribution and storage in terrestrial compartments (vegetation, soils, snowpacks and glaciers) and transfer of terrestrial Hg to the AO via riverine transport and coastal erosion.

Vegetation Hg

Vegetation uptake of atmospheric Hg(0) is a dominant source of Hg in vegetation[68,122] and soils[25,122] (through transfer when plants die) in the Arctic tundra. Pronounced Hg concentration differences exist both within and among different vegetation functional groups (lichen, mosses, and vascular plants) in the Arctic (Table S3): lichen (mean: 62±41 ng g^{-1}) and mosses (mean: 61±39 ng g^{-1}) generally show highest Hg concentrations, and lower Hg levels have been reported in vascular plants (mean: 10±5 ng g^{-1}). Arctic vascular plants show about three-times lower Hg concentrations than globally averaged vascular foliar (leaves and needles) concentrations (mean: 34±21 ng g^{-1})[123]. Arctic vegetation Hg data are still relatively sparse and large uncertainties exist in regard to spatiotemporal variability. Cryptogamic vegetation (which include lichen and mosses) show substantially higher Hg concentrations than vascular plants, and high variability is reported in Arctic lichen Hg concentrations (19−186 ng g^{-1}) (Table S3) due to differing deposition sources and pathways[124]. Lichens, as important forage substrates, can be potentially important Hg sources in caribou and other Arctic herbivores[124]. Hg concentrations ranging from 20-195 ng g^{-1} are reported [125,126] in mosses. Lichen and mosses have a large representation in Arctic vegetation communities, which leads to relatively high bulk vegetation Hg concentrations (mean: 49±37 ng g^{-1}) in the Arctic[122] (Table S3). One study[122] calculated tundra to contain aboveground standing Hg biomass

pools of 29 μg m^{-2} and a boreal forest study[127] showed a foliar Hg pool of 21 μg m^{-2} (Pallas, Finland). These northern standing biomass Hg pools are surprisingly similar in magnitude to foliar Hg biomass of lower-latitude forests with much longer growing seasons (15-45 μg m^{-2})[68,122,127].

Soil Hg

Arctic soils, a globally important Hg reservoir, have accumulated atmospheric Hg over millennia with anthropogenic Hg mostly confined to the surface layer[130]. Soil Hg can be released to surface waters via river runoff and coastal erosion or re-emitted to the atmosphere[68,128,129]. Higher Hg concentrations in active-layer (seasonally thawing and freezing) surface soils (65 ng g^{-1}, median) than deeper mineral (permafrost) horizons (48 ng g^{-1}, median) are primarily reported from soil profiles in Alaska[130], Svalbard[131] and the Western Siberian Lowlands[129] (Fig. 2a-b, Table S4). The Hg enrichment of surface soils highlights atmospheric Hg deposition as a major source[25,68,122]. Hg stable isotopes reveal that atmospheric Hg(0) vegetation uptake is the major deposition pathway in the Arctic Coastal Plain of Alaska, accounting for 70% (56-81%, interquartile range (IQR)) of Hg in organic surface O-horizons, 54% (43-62%, IQR) in A mineral horizons, and 24% (14-34%, IQR) in B horizons[25,68]. Geogenic source contributes 20% (A horizons) to 40% (B horizons)[25,68] Hg in mineral soils of Alaska. Oxidized Hg deposition during AMDEs is a minor contribution (<5%) to all soil horizons[68,130].

The Northern Hemisphere permafrost region 0-1 m soil Hg pool has been estimated to be 184 Gg (136–274 Gg, 25% confidence interval (CI))[130], 240 Gg (110–336 Gg, IQR)[129], and 755±301 Gg (95% CI)[128]. Along a Western Siberian Lowland transect, the 0-1 m soil Hg pool increases with latitude from 0.8 mg m^{-2} (56° N) to 13.7 mg m^{-2} (67° N), suggesting significant re-emission loses of soil Hg in the sub-Arctic[129]. The 0-3 m soil Hg pool estimates range from 597 Gg (384–750 Gg, IQR)[129] to 1656±962 Gg (95% CI)[128]. Alaska observations represent the largest share (50%) of the soil Hg data collected, but only cover 7% of the Northern Hemisphere permafrost region (Fig. 2a-b). To overcome the lack of spatially distributed Hg soil data, studies extrapolate limited observations of mercury to carbon ratios (Hg/C) in Arctic soils[128-130] to the entire Arctic region using high-resolution soil carbon maps[132]. The highest permafrost soil Hg estimate[128] is likely biased high; the application of elevated deeper mineral permafrost soil Hg/C ratio (1,600 ng g^{-1}) observed in northern Alaska (due to higher geogenic Hg levels) than elsewhere[68,130] to the entire Arctic[128] led to systematic overestimation of organic surface soils Hg content[129,130]. Best estimates for the Arctic soil Hg pool are ~49 Gg for 0-0.3 m (surface soils), ~212 Gg for 0–1 m (active layer soils), and ~597 Gg for 0–3 m, averaging the two Arctic soil Hg pool inventories based on whole-Arctic literature surveys and western Siberia data[129,130].

Snowpack Hg

With winter lasting about two-thirds of the year (September-May), the snowpack is a major substrate for atmospheric Hg exchange with Arctic ecosystems[1]. Unique physical and chemical cryospheric processes enrich Hg concentrations in polar snow (1-1,000 ng L^{-1} in Arctic snow; Table S7)[133] compared to lower latitude locations (1-~40 ng L^{-1})[134-137]. Frost flowers on sea ice[119,138,139], surface hoar crystals[140], and diamond dust[141] have elevated Hg concentrations (commonly 50-200 ng L^{-1} with values up to 1,200 ng L^{-1})[141]. Sea ice is a major source of reactive halogens to snowpacks and ambient air[70,142] that oxidize Hg(0) in air during AMDEs and can stabilize Hg in snow[106,108,133]. Hg stabilization in snow can arise from suppressed Hg(II) photo-reduction[143] and enhanced Hg(0) re-oxidation[144] by halogens in snowpacks, including in interstitial air[88] and at the stage of snowmelt[106,143]. Consequently, higher Hg concentrations are measured in snow at coastal locations (5-~200 ng L^{-1}; Svalbard, Alert, Utqiaġvik, and Greenland)[86,106,108107,145,146] than inland sites (0.5-5 ng L^{-1}; Toolik Lake, Alaska, Mt. Oxford and Agassiz, Canada, and Summit Station, Greenland)[68,74,147].

A large fraction (40-90%)[133] of snowpack Hg is re-emitted by photo-reduction, which depends on factors like halide and particulate matter content of snow, snowfall frequency, snow temperature, solar radiation, snowpack ventilation and upward latent heat flux[133,146,148-151]. However, due to relatively elevated snowpack Hg deposition rates in otherwise pristine locations a significant amount of Hg is retained, especially in coastal and marine regions[80,124]. A snowpack study from interior Alaska showed that the tundra snowpack is less prone to Hg(0) emissions than previously estimated[74]. During the spring freshet, Hg accumulated in snow and ice is: re-emitted during snow metamorphism and melt, exported to freshwaters or the marine system (40-80%, coastal Alaska), or incorporated into ecosystems by sorption to soil or vegetation surfaces[106]. Early snow melt includes an "ionic" pulse of major elements and elevated Hg concentrations (3-30 ng L^{-1})[106,145]. GEM-MACH-Hg simulation estimated an Arctic terrestrial seasonal snowpack Hg loading of 39 (35–42) Mg, and mean meltwater ionic pulse Hg concentrations that are generally lower in North America (< 10 ng L^{-1}) than in Eurasia (> 20 ng L^{-1}) due to differences in Hg deposition rates[80].

Glacial Hg

Glaciers mobilize Hg (dissolved and particulate) downstream via seasonal thaw and net ice mass wastage. The Hg in glacier-fed streams comes from anthropogenic and natural sources, including atmospheric deposition to snow, and erosion from bedrock. High-latitude glacier ice formed in the 19-20th centuries is enriched in Hg by factors of 2–15 relative to pre-industrial ice[28,152-154]. Upscaling an ice core-based estimate of the median Hg concentration (0.8 ng L^{-1})[28,152-1541] and using current estimates of glacier ice

volume[155], the mean size of the Arctic glacial Hg pool is estimated at 2415±22 Mg (~97% in Greenland). Based on spaceborne, gravity-based assessments of mass wasting rates[156,157] and ice-core Hg data, melting Arctic glacier ice releases 400±7 kg y^{-1} of Hg (~60% from Greenland). While total Hg levels in en- or supra-glacial ice are typically <1 ng L^{-1}, concentrations in sub- or pro-glacial streams fed by subglacial drainage can be 10-100s times larger, depending on catchment geology, owing to high particulate Hg loads (Table S5). A new study[158] reporting dissolved Hg levels of 44-351 ng L^{-1} in a west Greenland river presently stands as an outlier, calling for further confirmation. Typical Hg concentrations in bulk suspended particles carried by glacial streams are 5 to >500 ng g^{-1} [16,159-161], and estimated total Hg yields from most glacier-fed catchments are 0.03-3.88 g km^{-2} y^{-1} in basins with 21-82% glacier coverage, but a few have yields >10 g km^{-2} y^{-1} (Fig. 2d, Table S5). For Greenland, multiplying riverine particulate Hg concentrations[162] by estimated sediment exports yields[163] a total annual output of ~40 Mg y^{-1} Hg, far in excess of Hg releases from melting ice. Run off from Greenland mostly discharges into adjacent seas (>90%), with the remainder into the AO. Most glacierized catchments are in Greenland, the CAA and Svalbard[164], and thus outside the large mainland watersheds for which Hg fluxes are monitored[7,165]. Presently, the limited number of glacial rivers sampled (~10% in Table S5) and wide range of Hg levels and fluxes in these rivers make glacial Hg flux estimates uncertain.

Riverine Hg

Rivers mobilize and carry Hg from soils, snow, ice and released from permafrost and bedrock to freshwater ecosystems and the oceans. A strong coupling between Hg export and both water discharge and particle loadings suggests that hydrology and soil erosion are key drivers of Arctic riverine Hg export[7,165,166]. Over 90% of annual Hg export from large Arctic rivers occurs in spring/early summer, attesting to the importance of snowpack melt to riverine Hg[7,165,167-169] (Fig. 2). Hg:C ratio was observed to be 2-3 times higher in spring waters from western Siberia rivers compared to summer and fall[167], reflecting runoff of wintertime accumulated Hg deposition in snow. During the spring freshet, the ground is still frozen. Percolation through soil is thus not a major Hg source, but surface soil entrainment by overland flow and river bank erosion are [106]. Terrestrial contributions increase through summer as the ground thaws, leading to a minor second peak in Hg exports from some rivers during late summer or fall[165,167]. Mercury in snowmelt and surface soils released during spring likely originates mainly from recent atmospheric deposition, while later releases have larger, as yet unquantified, shares from legacy Hg deposition and natural sources[68,74,93,130,167]. Groundwater is important for some Arctic rivers (such as Yukon[170]), but its magnitude as a Hg source is unknown.

Local soil permeability, organic carbon content, glacial history, and vegetation cover all affect Hg storage and retention, making permafrost thaw contributions to riverine Hg exports difficult to quantify[171,172]. About 5% of Hg in Arctic soils is stored in regions with ice-rich permafrost susceptible to developing hillslope thermokarst features, like retrogressive thaw slumps, which can quickly mobilize vast amounts of particulate Hg into rivers[14]. Gradual thaw may also enhance particulate Hg export in streams, especially in the sporadic permafrost zone[167].

Total Hg concentrations vary by four orders of magnitude across Arctic watercourses (0.17−1,270 ng L^{-1}; Supplementary Table S5). The highest reported Hg levels are in streams affected by retrogressive thaw slumps (max. 1,270 ng L^{-1})[14], in ephemeral snowmelt-fed streams from coastal Alaska (max. 80 ng L^{-1})[93,106] where halogens likely drive enhanced Hg oxidation in air and retention in snow[108,144], and in turbid glacier-fed rivers (max. 74 ng L^{-1}) during peak discharge[16,160]. In rivers with large watersheds (>10^5 km^2), Hg concentrations are between 0.4 and 27 ng L^{-1} (median: 4.80 ng L^{-1}; Supplementary Table S5) with above 10 ng L^{-1} concentrations reported in northwestern North America (Yukon and Mackenzie watersheds) and Russia (Severnaya Dvina and Katun rivers). While tributaries to the Yukon and Mackenzie rivers are relatively pristine, the Katun River (Ob' watershed; max. 300 ng L^{-1}) flows over Hg-enriched bedrock[173], and the Severnaya Dvina River (5-21 ng L^{-1}) is locally impacted by Hg contamination around Archangelsk[174]. The share of particulate Hg varies between 29 and 60% across most Arctic rivers, but exceeds 85% in some glacier-fed streams[16,17].

Annual riverine Hg yields (average: 2.81 µg m^{-2}; median: 1.76 µg m^{-2}) in the Arctic exhibit large variations between watersheds (0.03−98.5 µg m^{-2}; Table S5), with 68% estimates between 0.9 and 4.4 µg m^{-2}. Higher river Hg yields are generally observed for rivers in western Eurasia and North America, with lower yields in Greenland, the CAA and western Hudson Bay (Fig. 2d). This pattern is broadly consistent with atmospheric Hg deposition across the Arctic (Figs. 1c and 3c). Watersheds on the AO coast are estimated to have the highest riverine Hg yields, driven by their high AMDE-led snowpack Hg loadings[7,80,93,106] (Fig. 2d).

Comparison between observation-based Hg exports from major Arctic rivers (Yenisei, Lena, Ob', Pechora, Severnaya Dvina, Kolyma, Mackenzie and Yukon draining about 70% of pan-Arctic watershed extending up to 45^0 N) and modeled (ensemble) Hg deposition reveals that river Hg exports are strongly positively correlated (r = 0.87) with their watershed Hg deposition components north of 60^0 N (Fig. S2; Table S6). Correspondingly, river Hg yields increase with increasing watershed proportions north of 60^0 N (Fig. 1d; Table S6). These results suggest greater re-emission[129] and/or sedimentation occurring of deposited Hg at latitudes south of 60^0 N. Additionally, river Hg yields are higher from the watersheds with greater Hg deposition rates (> 60^0 N), driven by proximity to Hg emission and presence of dominant

deposition pathways (Figs 1c and 2c; Table S6). The observation-based[7,165] total Hg export from the eight largest Arctic rivers (23.6 Mg y^{-1}) is about half of the modeled annual Hg deposition (47.6 Mg y^{-1}) and comparable to summertime (25.2 Mg y^{-1}) or snow cover period (22.4 Mg y^{-1}) Hg deposition in these watersheds north of 60^0 N (Table S6).

Observation-based estimates of annual Hg export from pan-Arctic rivers have converged on the range between 37[165] and 44[7] Mg y^{-1}, with eight major rivers exporting about 50% of the Hg. Much of this Hg is discharged directly to the AO (41±4 Mg y^{-1}), with 2-3 Mg y^{-1} entering Hudson and Baffin bays. Applying measured snowpack Hg export rate of ~50% (40-80%)[106] to the modeled end of season snowpack Hg loading (39 Mg y^{-1})[80] in the Arctic (north of 60^0 N) suggests that snowpacks supply up to half of the pan-Arctic river Hg export, the balance being derived from active layer surface soils. This finding is in line with observations of roughly equal amounts of dissolved and particulate Hg in river runoff to the ocean[7].

Future Arctic riverine Hg exports will be impacted by Arctic warming through accelerated permafrost thaw, glacier melt, increased rainfall, shorter snow cover seasons, and wildfire-related soil erosion. Glacial discharge is forecasted to increase across much of the Arctic until the mid-21st century; Greenland will become the dominant source thereafter, while outflow from smaller glaciers and ice cap will decline[175-177178]. These trends will likely be reflected in glacier-fed riverine Hg exports. Permafrost will also likely contribute more Hg to rivers via enhanced water percolation through a deepening active layer, and slump development along stream banks[167,171,179]. With unconstrained fossil fuel burning, terrestrial Hg model simulations for the Yukon River project a doubling of Hg(II) export by 2100, and a tripling by 2200[15]. However, thaw processes vary widely across ice-rich and ice-poor permafrost, making pan-Arctic projections more difficult and highlighting the need to quantify thaw-induced Hg releases in different settings. Understanding the sensitivity of small watershed Hg fluxes to change is especially important given their prevalence along Arctic coastlines.

Coastal erosion Hg export

Arctic coastal erosion rates are among the highest in the world because of long reaches of unlithified glacial drift in elevated bluffs, rapid sea-level changes, and exposed ground ice susceptible to the action of wind, water, and thermoerosion[180-182]. The Hg mass entering the ocean can be estimated from Arctic soil Hg concentrations in permafrost soils including the active layers compiled from the literature (REF [130,183,184] and references therein; REF[129], excluding a southern, non-permafrost site; Table S4), and eroding soil mass based on soil volumes from the Arctic Coastal Dynamics Database[185] (Table S7). Most soil Hg data are from inland tundra sites; additional sampling of coastal soils is needed to confirm their similarity to inland soils. Using the mean soil Hg concentration of 66.1±52.3 ng g^{-1} dry weight, the estimated annual

erosional Hg flux is 39±30 Mg y^{-1} (median 32 Mg y^{-1}; 18-52 Mg y^{-1}, IQR) (Table S7). The Eurasian Arctic, where erosion rates are highest, contributes 89% of the Hg flux. Calculated coastal erosion flux uncertainty only reflects the variability in soil Hg concentrations, not erosion mass.

Coastal erosion is increasing in many Arctic areas and is now higher than at any time since observations began 50-60 years ago because of interacting climatic, oceanographic and geomorphological factors[180,186]. A projected future increase in rates of coastline erosion[180,185] will contribute more Hg to the ocean.

Marine mercury

The Hg cycle in the AO is the key link between anthropogenic emissions and releases, Arctic marine biota and human exposure. Although efforts to understand the AO Hg cycle were historically hindered by a lack of data[187-190], coordinated efforts (such as GEOTRACES) since 2015 have made the AO one of the most sampled ocean basins with ~2000 total Hg seawater observations[19-22,191-194] (Fig. 3a).

The AO has unique and complex hydrography, distinguishing its Hg cycle from that of other oceans. The AO is covered by sea ice, affecting the air-sea Hg exchange. Almost completely surrounded by land and over half underlain by continental shelf, the AO receives a larger river discharge relative to its area than any other ocean. The freshwater inputs, traceable in the central AO, result in strong stratification[20,192,194]. Mercury enters the AO via rivers and coastal erosion, atmospheric deposition, and through Atlantic and Pacific Ocean inflows, and is removed from the Arctic water column by evasion, sedimentation, and outflow to the Atlantic Ocean.

Overall, Hg concentrations measured in Arctic waters are somewhat higher than in the North Atlantic[193] and global ocean[195] (Fig. 3a). The AO is the only ocean where the highest water Hg concentrations reside in the surface waters (0.24±0.12 ng L^{-1}, 0-20 m, n=159)[195]. North Atlantic-sourced waters flowing into the Arctic are lower in Hg (0.15±0.07 ng L^{-1}, 200–500m, n=164) as are Arctic deep waters below 500 m (0.13±0.06 ng L^{-1}, n=369). There is no significant difference in Hg concentrations between the Nansen, Amundsen, Makarov and Canadian Basins. Higher Hg levels were observed in the CAA[21,188] and on the North-Eastern Greenland Shelf, but not at the Barents Sea Opening[20]. Mercury concentrations in the East Siberian and Chukchi shelf (< 200m) averaged 0.22±0.08 ng L^{-1} (n=74)[22,196].

Using all available mean seawater total Hg concentration data[21,22,24,187,191,192,194], the water column Hg budget is revised to 1870 Mg (distributed by depth as: 44 Mg (0-20m), 228 Mg (20-200m), 224 Mg (200-500m) and 1375 Mg (500m-bottom)). This estimate is lower than reported in previous AO Hg mass budget studies (2847-7920 Mg)[6,197], primarily as a result of being based on more high latitude water measurements.

While there is no long-term temporal dataset for AO seawater Hg concentrations, some studies suggest that AO Hg concentrations and distribution will likely be affected by climate change. Climate change-induced loss of sea ice (5–10% decrease/decade in annual mean sea ice extent[198,199]) might result in a net increase in evasion flux of Hg from water to air[5,6], through enhanced net Hg reduction[19] and higher open water surface area[5]. In parallel, higher primary productivity[200] could enhance the removal of Hg from surface waters with the particle settling flux.

Air-sea Hg(0) exchange

Measurements of Hg(0) concentrations in the AO are limited[19,22,109] but show elevated concentrations in upper ocean waters especially under sea ice (Fig. 3b). Air-sea exchange of Hg(0) is a diffusion process largely controlled by surface water Hg(0) and water turbulence. High resolution measurements of surface water Hg(0) indicate supersaturation in summer and fall resulting in a net sea to air flux[19,109]. Hg(0) evasion is higher in coastal areas and the CAA (~144 ng m^{-2} d^{-1})[189] than in the ice-free open ocean (<24 ng m^{-2} d^{-1})[19,109,110], and higher in summer than in fall[19,109].

Sea ice acts as a barrier to evasion[19,109], allowing Hg(0) to build up likely by biologically-mediated and dark redox processes (~10^{-7} s^{-1})[8,101,196,201-203] linked to organic carbon cycling at the ice-water interface. Reaching a steady state under sea ice likely takes months assuming no other losses. The elevated concentrations suggest the potential for a substantial release of Hg(0) during spring/summer sea-ice melt[109]. As a result, there is likely enhanced Hg evasion in spring/summer during ice melt, and models suggest that this and snowpack melt contribute to the elevated atmospheric Hg concentrations measured at coastal locations in late spring/early summer[34,48,78,80]. The timescale for surface water Hg(0) to return to open water concentrations is several weeks[19].

A net Hg(0) evasion (diffusion) flux of 24.9 Mg y^{-1} from sea to air is estimated for the AO based on measurements of open ocean water flux estimates (77 ng m^{-2} d^{-1})[19,109], and an open water area ranging from 10% in winter to 65% in summer. Further, release of Hg(0) from under sea ice during melt is added based on seasonal sea ice changes and under ice Hg(0) concentrations (2.9 Mg y^{-1}), reaching a total evasion of 27.8 Mg y^{-1}. This is comparable to estimates of 45.0 and 23.3 Mg y^{-1} from GEOS-Chem and GEM-MACH-Hg models, respectively, providing a best estimate of 32 Mg y^{-1} (range 23–45 Mg y^{-1}) based on measurements and models.

Sea ice Hg exchange

Arctic sea ice is central to the Arctic Hg cycle, as it regulates the air-sea exchange of volatile Hg species[19], and controls the amount of sunlight that penetrates the water column and thus the photo-

mediated transformations of Hg[204]. Moreover, sea ice traps, accumulates[23,205,206], and transports Hg across the AO[194]. When seawater freezes, it traps Hg dissolved in the water or bound to particles in the newly formed ice. Sea ice matures by rejecting salts and dissolved Hg into brine, a halide and Hg-rich, dense, cold phase[205,208]. This brine has a low freezing temperature, remains liquid, and pools into channels. Thus, brine expulsion can move Hg from the bulk ice to the underlying seawater, enriching it (1.05±0.52 ng L^{-1})[23] relative to the polar mixed layer (~0.3 ng L^{-1})[192]. The amount of particulate Hg is highly variable and depends on the turbidity of waters where the sea ice originally formed. For example, "dirty ice" formed near the coast in resuspended sediment-rich waters[207], is enriched in particulate Hg[206]. Particle-bound contaminants are less likely to move into the brine and remain in the ice[206]. As sea ice ages, it loses Hg through brine expulsion or move to the surface and form frost flowers[23,208,119], but it can also gain Hg from atmospheric deposition or adsorption on snow and frost flowers[139,140]. Mercury can re-enter brine channels from underlying waters and sediment. All these processes affecting sea ice Hg result in the wide range of concentrations reported, from 0.1-12 ng L^{-1} [19,23,205,206,209]. However, when only Central AO sea ice[19,23] is considered, the overall concentration and the variability within cores and across sites are consistent (0.61±0.29 ng L^{-1}). Using this mean Hg concentration and the mean sea ice volume for 2015 ($1.54x10^4$ km^3), the AO sea ice Hg reservoir is estimated as 9.2 Mg (range 3.5-14.6 Mg). Annually, 1.4±0.4 Mg y^{-1} of sea ice Hg is exported out of the AO (through Fram Strait), assuming an approximate sea ice export of 2400±640 km^3.

Ocean currents Hg exchange

Mercury enters the AO through ocean currents from the Atlantic Ocean (43±9 Mg y^{-1}, Fram Strait[20]; 6±4 Mg y^{-1}, Barents Sea Opening[20]), and the Pacific Ocean (6[20] Mg y^{-1}, 1–14[22] and 3.7-7.6[6] Mg y^{-1}, Bering Strait), and exits via the Fram Strait (54±13 Mg y^{-1})[20] and Davis Strait (19±8 Mg y^{-1})[20] into the Atlantic Ocean. Improved data[20] have well-constrained the total AO oceanic Hg inflow (55±7 Mg y^{-1}) and outflow (73±8 Mg y^{-1}), compared to previous estimates (46[197] and 53 (40–62)[6] Mg y^{-1}, inflow; 68[197] and 79 (49–122)[6] Mg y^{-1}, outflow). Observations consistently suggest a net Hg export from the AO to the North Atlantic Ocean (18-26.2 Mg y^{-1})[6,20,197], due to the relatively high Hg concentrations in the outflow (0.26±0.09 ng L^{-1}) compared to the inflow (0.16±0.06 ng L^{-1}) [20].

While a slightly increasing trend in water inflow from Bering Strait has been observed, the Fram Strait water exchange shows strong seasonal variability but small long-term changes[210], which suggests no future trend for ocean Hg exchange due to low water input from Bering Strait[211].

Water-sediment Hg exchange

Rivers and coastal erosion, ocean primary production and wind-blown dust deposition provide organic/inorganic particles to the AO that accumulates in marine sediments (490 and 134 Gg/y in shelf and deep basins, respectively[6,212,213]). The high affinity of Hg to particles and the drawdown of particles from the surface ocean provide an important mechanism for Hg settling and burial in the marine sediments on millennial time scales[214].

The highest particulate Hg concentrations in the AO are observed over the shelf (0.031±0.01 ng L^{-1}) followed by Eastern (0.019±0.008 ng L^{-1}) and Western (0.014±0.010 ng L^{-1}) basins, which are about 3 times higher than in the North Atlantic[22,191,214]. When normalizing to particle weight, the Hg concentration of the particles increases from the shelf (211±69 ng g^{-1}) to the central Arctic Ocean (1,484±467 ng g^{-1})[191] compared to up to 90 ng g^{-1} (36±27 ng g^{-1})[215] near the Mackenzie River and 240-1,080 ng g^{-1} in the offshore North Atlantic Ocean[215]. The AO sediments Hg concentrations are also higher in the deep basin (60.4±44.5 ng g^{-1}, n=70) compared to the shelf (28.9±22.0 ng g^{-1}, n=70)[191].

Using suspended particulate Hg concentrations and Th-234 radionuclide tracer measurements, Hg settling fluxes from surface waters to below 100 m of 34.7±15.6 ng m^{-2} d^{-1} (shelf) and 9.2±43.3 ng m^{-2} d^{-1} (deep basin) are estimated[191]. The central AO Hg settling flux has a high uncertainty because of very low particle export fluxes. Total Hg settling fluxes from the surface ocean waters (100 meters depth) of 122±55 (shelf) Mg y^{-1} and 7.2±17 Mg y^{-1} (deep basin) are estimated for the AO area considered in this Review.

Marine sediments exchange Hg with overlying seawater by sedimentation/resuspension and bi-directional diffusion of Hg species[6]. A recent Th-230 radionuclide tracer approach refined the deep basin Hg burial flux[216] to 3.9±0.7 Mg y^{-1}, compared to previous estimates (8 Mg y^{-1} and 3.5±3 Mg y^{-1})[6,191]. Higher Hg burial rates are estimated in shelf sediments (30 Mg y^{-1} and 20±14 Mg y^{-1})[6,191]. However, the shelf Hg burial flux is likely underestimated due to a lack of measurements in the inner shelf, where burial is expected to be higher[217]. New observations on the Siberian shelf suggest Hg burial rates of up to 75 Mg y^{-1} and that earlier estimates are biased low because of underestimated sediment density[217]. Using all available data[191,216,217] gives a revised shelf Hg burial flux of 42±31 Mg y^{-1} (n=114). Net benthic Hg diffusion flux from the AO sediments to the overlying water column is estimated at 5 Mg y^{-1} for both shelf and deep basins based on limited data[6], calling for further measurements especially in the deep basin.

Mercury mass balance

In the last decade, observations and modeling have advanced the understanding of AO Hg mass balance[6,7,20,34,78,191]. This review provides a revised AO and first terrestrial system Hg mass balance assessment in the Arctic (Fig. 4; Table S9).

The Hg mass balance developed in this Review suggests that presently annual atmospheric Hg deposition of 118±20 Mg y^{-1} to the Arctic terrestrial system is balanced by legacy Hg emissions from soils and vegetation (including wildfires) and riverine and erosional exports totaling 113±32 Mg y^{-1} (Table S9). Northward-flowing rivers import part of the ~62 Mg y^{-1} Hg deposited over watershed areas south of 60°N to the Arctic, which is not accounted in the above terrestrial Hg inputs. Riverine Hg inflow to the Arctic is presently unquantifiable, as riverine fluxes and export rates are mostly measured at river mouths only. Large pools of Hg (212 (184-240) Gg, 0-1m, > three orders of magnitude larger than any other reservoirs) have accumulated in active layer and permafrost soils[128-130], derived from thousands of years of atmospheric deposition. It is likely that Arctic warming led to increased releases of terrestrial Hg in recent decades by intensifying permafrost thaw[14,218], glacier melt[16,17], coastal erosion[197], wildfires[13,219], and river discharge[168]. However, observational data are currently insufficient to quantify these changes. Uptake of Hg(0) by vegetation/soils/snowpack is now thought to be the dominant Hg deposition pathway in the Arctic terrestrial ecosystems[68,74,93], which is currently underestimated in models[37]. Legacy Hg emissions from undisturbed tundra soils seem negligible[68], and are likely overestimated in models (6.5-59 Mg y^{-1}; Table S9). Finally, wildfire Hg emissions and its speciation from boreal forests are highly temporally variable and uncertain, and reported to be rising[56,63-66].

Previously, Hg inputs to the AO from atmospheric deposition (45-108 Mg y^{-1})[6,34,78,80], pan-Arctic river runoff (46-80 Mg y^{-1})[6,34,36,78], coastal erosion (15-32 Mg y^{-1})[6,34], and ocean current inflow (46-55 Mg y^{-1})[6,20,197] were estimated to be offset by evasion (33-99 Mg y^{-1})[6,34,80], ocean outflow (68-79 Mg y^{-1})[6,20,197] and sediment burial (28 Mg y^{-1})[6,191] fluxes. In contrast, the revised AO Hg inputs (204.5±27.3 Mg y^{-1}) exceed outputs (152.3±33.9 Mg y^{-1}) by 52.2±43.5 Mg y^{-1} (Table S9), and indicate that Hg removal from the AO ocean waters is currently underestimated. Shelf Hg burial flux is likely underestimated due to a lack of measurements in the inner shelf, where burial is expected to be higher[217] (arrow q, Fig. 4). Mercury settling in shelf regions could be subsequently transferred into the deep basin via hydrodynamic exchanges[220,221] (arrow r, Fig. 4). Recent observations on the Siberian shelf suggest that Hg burial rates of up to 75 Mg y^{-1} are possible[217], and that earlier estimates are biased low because of underestimated sediment density. Large observed shelf Hg settling of 122±55 Mg y^{-1} from surface waters[191] also indicates that the revised shelf burial flux (42±31 Mg y^{-1}) using all available data (n=114)[191,216,217] might be underestimated by up to 80±63.1 Mg y^{-1}, which is in the range of excess AO Hg input (52.2±43.5 Mg y^{-1}) found here. Riverine and erosional Hg exports to the AO are highly seasonal, primarily occurring during

spring freshet and summer months[7,165]. The fate of terrestrial Hg input in the AO is currently uncertain, and likely varies between watersheds due to differences in the reactivity of particulate organic carbon-bound mercury[36,194,222,223].

Summary and future perspectives

A quantitative understanding of the Arctic total Hg levels, movement pathways and mass balance is developed by integrating observations and modeling, in support of future effectiveness evaluation of the Minamata Convention. About 330 Mg Hg presently circulates in the Arctic atmosphere north of 60^0 N, primarily transported from distant global emissions sources (6000-9000 Mg y^{-1})[37], with small contributions from regional anthropogenic emissions (14 Mg y^{-1}) and re-emission of legacy Hg by wildfires (8.8±6.4 Mg y^{-1}) and by vegetation/soil evasion (24 (6.5-59) Mg y^{-1}). Annually, 118±20 Mg y^{-1} and 64.5±19.8 Mg y^{-1} of atmospheric Hg is deposited to Arctic terrestrial and marine environments, respectively.. Mercury deposited on land is stored in permafrost soils (597,000 Mg, 0-3 m), glaciers (2,415 Mg) and seasonal snowpacks (~39 (35–42) Mg). Rivers and coastal erosion respectively transfer 41±4 and 39 (18-52) Mg y^{-1} of terrestrial Hg to the AO reservoir (1,870 Mg). Oceanic inflows supply 55±7 Mg y^{-1} of Hg to the AO, while the outflow exports 73±8 Mg y^{-1} to the Atlantic Ocean. About 32 (23-45) Mg y^{-1} of Hg is lost from the AO by evasion to air, while sedimentation buries 42±31 Mg y^{-1} (likely significantly underestimated) and 3.9±0.7 Mg y^{-1} of oceanic Hg in continental shelves and the deep basin, respectively.

Research advances in following key areas is needed to improve the understanding of the processes controlling the present and future Arctic Hg cycling. To better quantify anthropogenic Hg emissions in the Arctic, improved information on Hg regional sources such as activity data on quantities of fuels and raw materials used at major point sources, and their associated Hg content, as well as that of their products is necessary. Information on the locations, quantities and practices involved in waste disposal in the Arctic, and waste characteristics would allow better estimates, not only of Hg emissions but also of the releases of a range of environmental contaminants. Mercury measurements in biome-specific wildfires including peat fires, and improved methods for wildfire Hg emission inventories including global warming impacts are required. Mechanistic modeling schemes for vegetation Hg uptake from the atmosphere incorporating plant physiology, redox chemistry and environmental variables are needed. The role of sea ice/snow dynamics and photo-chemistry in marine Hg redox processes needs to be better understood. More air-surface Hg flux observations from inland, coastal and marine sites would help to develop mechanistic knowledge of atmosphere-surface and sediment-ocean Hg exchange processes, and their climate warming effects.

Mercury releases from thawing Arctic permafrost into rivers and from eroding coastlines into the ocean depend on factors such as soil organic carbon, geomorphology, hydrology, and ground ice, which vary widely across the Arctic. Thus, spatially-resolved permafrost soil Hg inventories are needed to understand and quantify Hg releases to downstream and coastal ecosystems across different regions and thaw regimes. Improved estimates of glacial Hg reservoir and its outflow across a range of catchment sizes and geological settings, particularly where local ecosystem impacts could be large (such as productive fjords), and projections of glacial meltwater discharges into lakes and the ocean are required to forecast impacts to aquatic ecosystems.

Further application of Hg stable isotopes might better constrain the processes influencing cycling of Hg through the air-soil-river pathway into the AO and marine food webs under present and future conditions. Applying extensive knowledge of the radiocarbon ages and soil profile sources of dissolved and particulate organic carbon in Arctic rivers might help elucidate the natural:anthropogenic source attribution of dissolved and particulate Hg fluxes into the AO. Seasonal observations of suspended sediment and dissolved Hg fluxes onto the shelf and in the central AO are needed to understand and quantify the fate of pulsed terrestrial Hg inputs. Finally, integrated atmosphere-land-ocean biogeochemical Hg models are needed to simulate the link between terrestrial Hg deposition and its export, and the impacts of concurrent changes in global climate and Hg emissions on Arctic Hg cycling.

Figure 1. | Atmospheric Hg distribution in the Arctic. a| Model ensemble (DEHM, GEM-MACH-Hg, GLEMOS, GOES-Chem) simulated (this Review) annual average surface air gaseous elemental mercury (Hg(0)) concentrations in 2015. **b**| Annual mercury (Hg) wet deposition flux in 2015. **c**| Annual Hg total deposition in the Arctic in 2015. Circles show observations in the same color scale. The blue lines delineate major pan-Arctic river watersheds. Air concentrations and wet deposition observations are from ECCC-AMM[83], AMNet[84], EMEP[85] and REF[224], and total deposition observation is from REF [29].

Figure 2. | **Distribution of total Hg in Arctic soils, wintertime deposition and rivers. a**| Mean mercury (Hg) concentrations of active layer soils within 0-1 m depth. **b**| Mean Hg concentration of permafrost layer soils within 0-1 m depth. Symbols in Figs. a-b represent the soil type with squares for organic soils, circles for mineral soils and triangles for combined organic/mineral soils **c**| Wintertime (September-May) model ensemble simulated Hg deposition to snowpack. Observations are shown in circles **d**| Annual river total mercury (THg) yields (annual riverine THg mass flux to the Arctic Ocean divided by watershed area) for pan-Arctic watersheds. Larger watersheds (> 10,000 km^2) are delineated where possible, while smaller watersheds are represented by symbols. Solid colored watersheds and squares represent measured THg yields (n=32) reported in REF[7,16-18,107,162,165,169,173,225-228]. Hatched watersheds and circles are THg

yields (n=100) modelled in REF[7]. Numbered watersheds are: 1) Amguema, 2) Palyavaam, 3) Bolshoy Anyuy, 4) Indigirka, 5) Yana, 6) Omoloy, 7) Olenek, 8) Anabar, 9) Khatanga, 10) Katun, 11) Taz, 12) Pur, 13) Nadym, 14) Pechora, 15) Mezen, 16) Onega, 17) Ponoy, 18) Varzuga, 19) Nyzhny Vig (Sor), 20) Kem, 21) Tana, 22) George, 23) À la Baleine, 24) Povungnituq, 25) Arnaud, 26) Aux Feuilles, 27) Koksoak, 28) Grande Rivière de la Baleine, 29) La Grande Rivière, 30) Eastmain, 31) Rupert, 32) Nottaway, 33) Moose, 34) Albany, 35) Attawapiskat, 36) Winisk, 37) Severn, 38) Hayes, 39) Churchill, 40) Seal, 41) Thlewiaza, 42) Ferguson, 43) Thelon, 44) Back, 45) Ellice, 46) Coppermine, 47) Hornaday, 48) Anderson, 49) Peel, 50) Noatak, 51) Kobuk. For rivers with multiple yield estimates, only the estimate for the most recent time period is shown. **e**| Repeat images during spring melt in Utqiaġvik (formerly Barrow), Alaska during a typical spring melt. In a matter of a few weeks the tundra surface goes from completely snow covered to a wet vegetation and soil surface exposed to continuous sunlight.

Figure 3. | Spatial distribution of Hg in the Arctic Ocean. **a**| Synoptic pan-Arctic transect of total Hg concentrations during the 2015 GEOTRACES cruises (ng L^{-1})[22,191,194]. The insert map shows the transect (red band) and available Hg observations (blue dots). **b**| Surface water Hg(0) concentrations (ng L^{-1}) in the Arctic Ocean during a summer (left[109]) and fall (right[19]) cruise. Grey areas indicate ice-covered water. The area indicated with a punctuated line represents the outflow region from the Mackenzie River Basin. Ocean currents transport Hg via waters entering the AO from the Atlantic Ocean (235±31.7x10^3 km^3 y^{-1}, Fram Strait; 72.9±38.0x10^3 km^3 y^{-1}, Barents Sea Opening), and the Pacific Ocean (22.2±22.2x10^3 km^3 y^{-1}, Bering Strait), and exiting the AO through the Davis Strait (66.6±22.2x10^3 km^3 y^{-1}) and Fram Strait (273±114x10^3 km^3 y^{-1}) into the Atlantic Ocean[210,229].

Figure 4 | Arctic Hg inter-compartmental annual fluxes and reservoir budgets. Best estimates (black numbers) and uncertainties in terrestrial and oceanic Hg annual fluxes (identified by arrows with letters) are: anthropogenic (a, 14 Mg y^{-1}), natural and legacy soils/vegetation volatilization (b, $24^{+35.1}_{-17.5}$ Mg y^{-1}), wildfires (c, 8.8±6.4 Mg y^{-1}), and ocean (d, 32^{+13}_{-9} Mg y^{-1}) emissions; terrestrial (e, 118±20 Mg y^{-1}), and ocean (f, 64.5±19.8 Mg) deposition; coastal erosion (g, 39^{+13}_{-11} Mg y^{-1}), river (h, 41±4 Mg y^{-1}), ocean (i, 55+7 Mg y^{-1}), and benthic shelf (j, 5 Mg y^{-1}) imports; sea ice (k, 1.4± 0.4 Mg y^{-1}), ocean (l, 73±8 Mg y^{-1}), shelf burial (m, 42±31 Mg y^{-1}) and deep ocean burial (n, 3.9±0.7 Mg y^{-1}) exports; and in-ocean shelf (o, 122±55 Mg y^{-1}) and deep ocean (p, 7.2±17 Mg y^{-1}) downward fluxes from surface waters. Best estimates (black numbers) and uncertainties for Hg budgets in reservoirs are: atmosphere (330^{+30}_{-40} Mg), glaciers (2,415±22 Mg), snowpacks (39^{+3}_{-4} Mg), soils (surface, 0-0.3 m: 49±13 Gg; active layer, 0-1 m: 212±28 Gg; permafrost, 0-3 m: 597 Gg), and Arctic Ocean (44±22 Mg, 0-20 m; 228±112 Mg, 20-200 m;

224±106 Mg, 200-500 m; 1,375±616 Mg, 500 m and deeper). Red arrows indicate unknown Hg fluxes of burial in estuaries and inner shelf (q), transport from shelf to deep Arctic Ocean basin (r), and benthic deep basin (s) fluxes (identified in this Review). Arctic Ocean sediments Hg concentrations are 28.9±22.0 ng g^{-1} in shelf and 60.4±44.5 ng g^{-1} in deep basin. Arctic land is defined as region north of 60° N and the Arctic Ocean is defined as the central basin, and Barents, Kara, Laptev East Siberian, Chukchi and Beaufort Seas, (94.5×10^5 km^2, total ocean surface area; 53% shelf). The values of Hg fluxes and budgets are based on multi-model ensemble simulations and peer-reviewed literature (this Review).

Box 1 | The role of speciation in Arctic mercury cycling

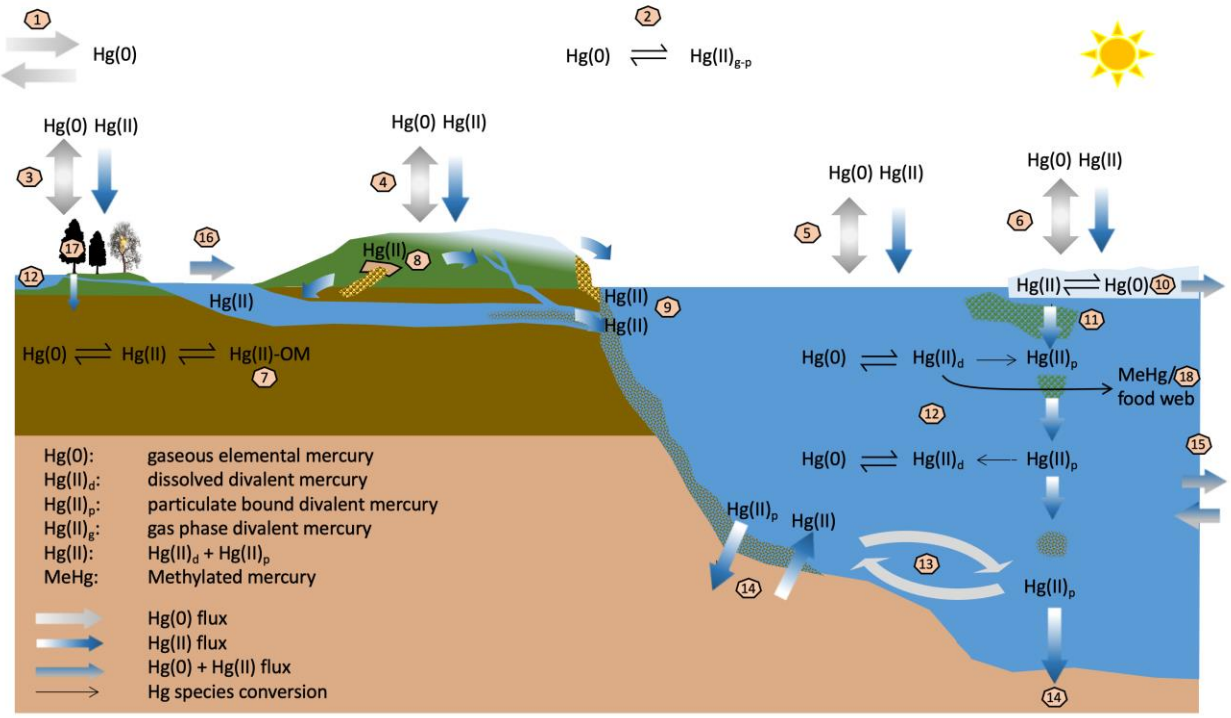

Mercury (Hg) in the Arctic occurs in different chemical forms that are subject to (photo-)chemical and biologically-mediated transformations[67,230,231]. Mercury is transported to and from the Arctic through air (*1*)[232], rivers (*16*)[7] and ocean currents (*15*)[20]. The atmospheric Hg pool *(2)* consist of gaseous elemental

Hg (Hg(0); >95%) and oxidized divalent Hg (Hg(II))[67], and it exchanges with vegetation, soil, snow, ice and seawater *(3-6)*[6] primarily through dry deposition of Hg(0) and Hg(II), wet deposition of Hg(II), and evasion of Hg(0)[19,37,68,93]. Transfers of Hg between terrestrial, aquatic and ice/snow reservoirs are controlled by light, organic matter complexation, and microbial activity[1]. Mercury stored in terrestrial reservoirs, primarily as particulate Hg(II), is mobilized by snow/ice melt[16,17,106], permafrost thaw[14], bedrock weathering, soil erosion and surface runoff (*7, 8, 10, 12*); and can be transported into wetlands, lakes and riverbeds or onto marine shelves (*14*)[165,167,168,183]. Once it reaches the Arctic Ocean, Hg is distributed by currents (*13)*[20,36], settling (*11, 14*), biological uptake and release (*11, 18*), and remineralization (*12*)[6,191,233]. A fraction of Hg(0) and Hg(II) can be converted to methylmercury (MeHg) (*18*)[231,234,235]. Unlike in other reservoirs, MeHg can in ocean waters be the dominant form of Hg, most prominently observed in the deeper parts of the ocean[192]. MeHg is a neurotoxic that bioaccumulates and biomagnifies in food webs often reaching high levels in top predators particularly in aquatic environments where food webs are longer than in terrestrial systems (*18*)[1]. Phytoplankton uptake is the main pathway of MeHg into aquatic food webs[236]. A distinctive feature of the Arctic Ocean is the presence of a large water MeHg peak overlapping with maximum phytoplankton activity[187,192], resulting in favorable conditions for uptake by food webs. MeHg concentration in phytoplankton is 10^4 or more times higher than in water although uptake is species and conditions dependent[237,238]. Hg concentration continues to increase at each subsequent trophic level in the food web culminating in long-lived predatory fish and marine mammals (including amphibious animals such as polar bears) exceeding Hg concentrations 10^7 times that of seawater[1].

Author contributions

A.D. designed, coordinated and led the study and manuscript writing, editing and revising. All authors (listed in alphabetical order) contributed to analyzing data, writing and/or conducting model simulations of specific sections, developing Arctic mercury mass balance, key points and future perspectives, and revising manuscript. K.A.S.P. and C.Z. also contributed to overall editing and formatting.

Acknowledgements

H.A. acknowledges Noelle E. Selin and the use of the Svante cluster provided by the Massachusetts Institute of Technology's Joint Program on the Science and Policy of Global Change. M.J. acknowledges funding from the Swiss National Science Foundation grant PZ00P2_174101. R.P.M. acknowledges funding from the US National Science Foundation Polar Programs grant 1854454. D.O acknowledges funding from the US National Science Foundation (DEB # 2027038 and AGS # 1848212). A.T.S.

acknowledges support from the US National Science Foundation (OCE # 2023046). Authors acknowledge the Arctic Monitoring and Assessment Programme (AMAP) for organizing the 2021 Arctic mercury assessment process that provided the basis for this review. Finally, authors acknowledge the Atmospheric Mercury Network (AMNet), European Monitoring and Evaluation Programme (EMEP) and Environment and Climate Change Canada-Atmospheric Mercury Measurement Network (ECCC-AMM) and their contributing scientists for the provision of mercury measurement data.

Competing interests

The authors declare no competing interests.

References

1. AMAP. AMAP Assessment 2011: Mercury in the Arctic. xiv + 193 pp. (Oslo, Norway, 2011).
2. Dietz, R. *et al.* Current state of knowledge on biological effects from contaminants on arctic wildlife and fish. *Sci. Total Environ.* **696**, 133792 (2019).
3. Environment, U. Global Mercury Assessment 2018. (Geneva Switzerland, 2019).
4. Basu, N. *et al.* A State-of-the-Science Review of Mercury Biomarkers in Human Populations Worldwide between 2000 and 2018. *Environ. Health Perspect.* **126**, 106001 (2018).
5. Chen, L. *et al.* A decline in Arctic Ocean mercury suggested by differences in decadal trends of atmospheric mercury between the Arctic and northern midlatitudes. *Geophys. Res. Lett.* **42**, 6076-6083 (2015).
6. Soerensen, A. L. *et al.* A mass budget for mercury and methylmercury in the Arctic Ocean. *Global Bigeochem. Cycles* **30**, 560-575 (2016).
7. Sonke, J. E. *et al.* Eurasian river spring flood observations support net Arctic Ocean mercury export to the atmosphere and Atlantic Ocean. *PNAS* **115**, E11586 (2018).
8. Qureshi, A., O'Driscoll, N. J., MacLeod, M., Neuhold, Y.-M. & Hungerbühler, K. Photoreactions of Mercury in Surface Ocean Water: Gross Reaction Kinetics and Possible Pathways. *Environ. Sci. Technol.* **44**, 644-649 (2010).
9. O'Driscoll, N. J. *et al.* Dissolved Gaseous Mercury Production at a Marine Aquaculture Site in the Mercury-Contaminated Marano and Grado Lagoon, Italy. *Bull. Environ. Contam. Toxicol.* **103**, 218-224 (2019).
10. Mason, R. P., Reinfelder, J. R. & Morel, F. M. M. Bioaccumulation of mercury and methylmercury. *Water Air Soil Pollut.* **80**, 915-921 (1995).
11. AMAP. AMAP Assessment 2021: Mercury in the Arctic. Summary for Policy-Makers. 16 pp. (Tromsø, Norway, 2021).
12. Clem, K. R. *et al.* Record warming at the South Pole during the past three decades. *Nat. Clim. Change* **10**, 762-770 (2020).
13. Kumar, A. & Wu, S. Mercury Pollution in the Arctic from Wildfires: Source Attribution for the 2000s. *Environ. Sci. Technol.* **53**, 11269-11275 (2019).
14. St. Pierre, K. A. *et al.* Unprecedented Increases in Total and Methyl Mercury Concentrations Downstream of Retrogressive Thaw Slumps in the Western Canadian Arctic. *Environ. Sci. Technol.* **52**, 14099-14109 (2018).
15. Schaefer, K. *et al.* Potential impacts of mercury released from thawing permafrost. *Nat. Commun.* **11**, 4650 (2020).

16. St. Pierre, K. A. *et al.* Drivers of Mercury Cycling in the Rapidly Changing Watershed of the High Arctic's Largest Lake by Volume (Lake Hazen, Nunavut, Canada). *Environ. Sci. Technol.* **53**, 1175-1185 (2019).
17. Søndergaard, J. *et al.* Mercury exports from a High-Arctic river basin in Northeast Greenland (74 degrees N) largely controlled by glacial lake outburst floods. *Sci. Total Environ.* **514**, 83-91 (2015).
18. Zdanowicz, C. *et al.* Snowmelt, glacial and atmospheric sources of mercury to a subarctic mountain lake catchment, Yukon, Canada. *Geochim. Cosmochim. Acta* **238**, 374-393 (2018).
19. DiMento, B. P., Mason, R. P., Brooks, S. & Moore, C. The impact of sea ice on the air-sea exchange of mercury in the Arctic Ocean. *Deep Sea Res. Part I* **144**, 28-38 (2019).
20. Petrova, M. V. *et al.* Mercury species export from the Arctic to the Atlantic Ocean. *Mar. Chem.* **225**, 103855 (2020).
21. Wang, K. *et al.* Subsurface seawater methylmercury maximum explains biotic mercury concentrations in the Canadian Arctic. *Sci. Rep.* **8**, 14465 (2018).
22. Agather, A. M., Bowman, K. L., Lamborg, C. H. & Hammerschmidt, C. R. Distribution of mercury species in the Western Arctic Ocean (U.S. GEOTRACES GN01). *Mar. Chem.* **216**, 103686 (2019).
23. Schartup, A. T., Soerensen, A. L. & Heimbürger-Boavida, L.-E. Influence of the Arctic Sea-Ice Regime Shift on Sea-Ice Methylated Mercury Trends. *Environ. Sci. Technol. Lett.* **7**, 708-713 (2020).
24. Kim, J. *et al.* Mass Budget of Methylmercury in the East Siberian Sea: The Importance of Sediment Sources. *Environ. Sci. Technol.* **54**, 9949-9957 (2020).
25. Jiskra, M., Sonke, J. E., Agnan, Y., Helmig, D. & Obrist, D. Insights from mercury stable isotopes on terrestrial–atmosphere exchange of Hg(0) in the Arctic tundra. *Biogeosciences* **16**, 4051-4064 (2019).
26. Blum, J. D., Sherman, L. S. & Johnson, M. W. Mercury Isotopes in Earth and Environmental Sciences. *Annu. Rev. Earth Planet. Sci.* **42**, 249-269 (2014).
27. Štrok, M., Baya, P. A. & Hintelmann, H. The mercury isotope composition of Arctic coastal seawater. *C.R. Geosci.* **347**, 368-376 (2015).
28. Zdanowicz, C. M. *et al.* Historical variations of mercury stable isotope ratios in Arctic glacier firn and ice cores. *Global Bigeochem. Cycles* **30**, 1324-1347 (2016).
29. Obrist, D. *et al.* A review of global environmental mercury processes in response to human and natural perturbations: Changes of emissions, climate, and land use. *Ambio* **47**, 116-140 (2018).
30. Dibble, T. S., Tetu, H. L., Jiao, Y., Thackray, C. P. & Jacob, D. J. Modeling the OH-Initiated Oxidation of Mercury in the Global Atmosphere without Violating Physical Laws. *J. Phys. Chem. A* **124**, 444-453 (2020).
31. Saiz-Lopez, A. *et al.* Photochemistry of oxidized Hg(I) and Hg(II) species suggests missing mercury oxidation in the troposphere. *PNAS* **117**, 30949 (2020).
32. Zhang, Y. *et al.* Observed decrease in atmospheric mercury explained by global decline in anthropogenic emissions. *PNAS* **113**, 526-531 (2016).
33. Angot, H. *et al.* Chemical cycling and deposition of atmospheric mercury in polar regions: review of recent measurements and comparison with models. *Atmos. Chem. Phys.* **16**, 10735-10763 (2016).
34. Fisher, J. A. *et al.* Riverine source of Arctic Ocean mercury inferred from atmospheric observations. *Nat. Geosci.* **5**, 499-504 (2012).
35. Fisher, J. A. *et al.* Factors driving mercury variability in the Arctic atmosphere and ocean over the past 30 years. *Global Bigeochem. Cycles* **27**, 1226-1235 (2013).
36. Zhang, Y. *et al.* Biogeochemical drivers of the fate of riverine mercury discharged to the global and Arctic oceans. *Global Bigeochem. Cycles* **29**, 854-864 (2015).
37. Zhou, J., Obrist, D., Dastoor, A., Jiskra, M. & Ryjkov, A. Vegetation uptake of mercury and impacts on global cycling. *Nat. Rev. Earth Environ.* **2**, 269-284 (2021).

38. Bishop, K. *et al.* Recent advances in understanding and measurement of mercury in the environment: Terrestrial Hg cycling. *Sci. Total Environ.* **721**, 137647 (2020).
39. AMAP & Environment, U. Technical Background Report for the Global Mercury Assessment 2018. Arctic Monitoring and Assessment Programme. viii + 426 pp including E-Annexes (Oslo, Norway & Geneva, Switzerland, 2019).
40. Outridge, P. M., Mason, R. P., Wang, F., Guerrero, S. & Heimbürger-Boavida, L. E. Updated Global and Oceanic Mercury Budgets for the United Nations Global Mercury Assessment 2018. *Environ. Sci. Technol.* **52**, 11466-11477 (2018).
41. De Simone, F. *et al.* Particulate-phase mercury emissions from biomass burning and impact on resulting deposition: a modelling assessment. *Atmos. Chem. Phys.* **17**, 1881-1899 (2017).
42. Kumar, A., Wu, S., Huang, Y., Liao, H. & Kaplan, J. O. Mercury from wildfires: Global emission inventories and sensitivity to 2000–2050 global change. *Atmos. Environ.* **173**, 6-15 (2018).
43. Friedli, H. R., Arellano, A. F., Cinnirella, S. & Pirrone, N. Initial Estimates of Mercury Emissions to the Atmosphere from Global Biomass Burning. *Environ. Sci. Technol.* **43**, 3507-3513 (2009).
44. Bozem, H. *et al.* Characterization of transport regimes and the polar dome during Arctic spring and summer using in situ aircraft measurements. *Atmos. Chem. Phys.* **19**, 15049-15071 (2019).
45. Law, K. S. *et al.* Arctic Air Pollution: New Insights from POLARCAT-IPY. *Bull. Ameri. Meteorol. Soc.* **95**, 1873-1895 (2014).
46. Monks, P. S. *et al.* Tropospheric ozone and its precursors from the urban to the global scale from air quality to short-lived climate forcer. *Atmos. Chem. Phys.* **15**, 8889-8973 (2015).
47. Weiss-Penzias, P. *et al.* Quantifying Asian and biomass burning sources of mercury using the Hg/CO ratio in pollution plumes observed at the Mount Bachelor observatory. *Atmos. Environ.* **41**, 4366-4379 (2007).
48. Durnford, D., Dastoor, A., Figueras-Nieto, D. & Ryjkov, A. Long range transport of mercury to the Arctic and across Canada. *Atmos. Chem. Phys.* **10**, 6063-6086 (2010).
49. Pithan, F. *et al.* Role of air-mass transformations in exchange between the Arctic and mid-latitudes. *Nat. Geosci.* **11**, 805-812 (2018).
50. Lee, M.-Y., Hong, C.-C. & Hsu, H.-H. Compounding effects of warm sea surface temperature and reduced sea ice on the extreme circulation over the extratropical North Pacific and North America during the 2013–2014 boreal winter. *Geophys. Res. Lett.* **42**, 1612-1618 (2015).
51. Pozzoli, L., Dobricic, S., Russo, S. & Vignati, E. Impacts of large-scale atmospheric circulation changes in winter on black carbon transport and deposition to the Arctic. *Atmos. Chem. Phys.* **17**, 11803-11818 (2017).
52. Dastoor, A. *et al.* Atmospheric mercury in the Canadian Arctic. Part II: Insight from modeling. *Sci. Total Environ.* **509-510**, 16-27 (2015).
53. Steenhuisen, F. & Wilson, S. J. Development and application of an updated geospatial distribution model for gridding 2015 global mercury emissions. *Atmos. Environ.* **211**, 138-150 (2019).
54. Friedli, H. R. *et al.* Mercury emissions from burning of biomass from temperate North American forests: laboratory and airborne measurements. *Atmos. Environ.* **37**, 253-267 (2003).
55. Webster, J. P., Kane, T. J., Obrist, D., Ryan, J. N. & Aiken, G. R. Estimating mercury emissions resulting from wildfire in forests of the Western United States. *Sci. Total Environ.* **568**, 578-586 (2016).
56. McLagan, D. S., Stupple, G. W., Darlington, A., Hayden, K. & Steffen, A. Where there is smoke there is mercury: Assessing boreal forest fire mercury emissions using aircraft and highlighting uncertainties associated with upscaling emissions estimates. *Atmos. Chem. Phys.* **21**, 5635-5653 (2021).
57. Giglio, L., Randerson, J. T. & van der Werf, G. R. Analysis of daily, monthly, and annual burned area using the fourth-generation global fire emissions database (GFED4). *J. Geophys. Res.: Biogeosci.* **118**, 317-328 (2013).

58. Giglio, L., Schroeder, W. & Justice, C. O. The collection 6 MODIS active fire detection algorithm and fire products. *Remote Sens. Environ.* **178**, 31-41 (2016).
59. Lizundia-Loiola, J., Otón, G., Ramo, R. & Chuvieco, E. A spatio-temporal active-fire clustering approach for global burned area mapping at 250 m from MODIS data. *Remote Sens. Environ.* **236**, 111493 (2020).
60. Amiro, B. D. *et al.* Direct carbon emissions from Canadian forest fires, 1959-1999. *Can. J. Forest Res.* **31**, 512-525 (2001).
61. Turetsky, M. R. *et al.* Wildfires threaten mercury stocks in northern soils. *Geophys. Res. Lett.* **33**, L16403 (2006).
62. Kohlenberg, A. J., Turetsky, M. R., Thompson, D. K., Branfireun, B. A. & Mitchell, C. P. J. Controls on boreal peat combustion and resulting emissions of carbon and mercury. *Environ. Res. Lett.* **13**, 035005 (2018).
63. AMAP. Impacts of short-lived climate forcers on Arctic climate, air quality, and human health. Summary for policy-makers. (Oslo, Norway, 2021).
64. Comeau, A. M., Li, W. K. W., Tremblay, J.-É., Carmack, E. C. & Lovejoy, C. Arctic Ocean Microbial Community Structure before and after the 2007 Record Sea Ice Minimum. *PLoS One* **6**, e27492 (2011).
65. Veira, A., Lasslop, G. & Kloster, S. Wildfires in a warmer climate: Emission fluxes, emission heights, and black carbon concentrations in 2090–2099. *J. Geophys. Res.: Atmos.* **121**, 3195-3223 (2016).
66. Walker, X. J. *et al.* Increasing wildfires threaten historic carbon sink of boreal forest soils. *Nature* **572**, 520-523 (2019).
67. Steffen, A. *et al.* Atmospheric mercury in the Canadian Arctic. Part I: A review of recent field measurements. *Sci. Total Environ.* **509-510**, 3-15 (2015).
68. Obrist, D. *et al.* Tundra uptake of atmospheric elemental mercury drives Arctic mercury pollution. *Nature* **547**, 201-204 (2017).
69. Wang, S. *et al.* Direct detection of atmospheric atomic bromine leading to mercury and ozone depletion. *PNAS* **116**, 14479 (2019).
70. Abbatt, J. P. D. *et al.* Halogen activation via interactions with environmental ice and snow in the polar lower troposphere and other regions. *Atmos. Chem. Phys.* **12**, 6237-6271 (2012).
71. Pratt, K. A. *et al.* Photochemical production of molecular bromine in Arctic surface snowpacks. *Nat. Geosci.* **6**, 351-356 (2013).
72. Toyota, K., McConnell, J. C., Staebler, R. M. & Dastoor, A. P. Air–snowpack exchange of bromine, ozone and mercury in the springtime Arctic simulated by the 1-D model PHANTAS – Part 1: In-snow bromine activation and its impact on ozone. *Atmos. Chem. Phys.* **14**, 4101-4133 (2014).
73. Marelle, L. *et al.* Implementation and Impacts of Surface and Blowing Snow Sources of Arctic Bromine Activation Within WRF-Chem 4.1.1. *J. Adv. Model. Earth Syst.* **13**, e2020MS002391 (2021).
74. Agnan, Y., Douglas, T. A., Helmig, D., Hueber, J. & Obrist, D. Mercury in the Arctic tundra snowpack: temporal and spatial concentration patterns and trace gas exchanges. *Cryosphere* **12**, 1939-1956 (2018).
75. Travnikov, O. *et al.* Multi-model study of mercury dispersion in the atmosphere: atmospheric processes and model evaluation. *Atmos. Chem. Phys.* **17**, 5271-5295 (2017).
76. Travnikov, O. & Ilyin, I. in *Mercury Fate and Transport in the Global Atmosphere: Emissions, Measurements and Models* (eds Robert Mason & Nicola Pirrone) 571-587 (Springer US, 2009).
77. Holmes, C. D. *et al.* Global atmospheric model for mercury including oxidation by bromine atoms. *Atmos. Chem. Phys.* **10**, 12037-12057 (2010).
78. Dastoor, A. P. & Durnford, D. A. Arctic Ocean: Is It a Sink or a Source of Atmospheric Mercury? *Environ. Sci. Technol.* **48**, 1707-1717 (2014).

79. Fraser, A., Dastoor, A. & Ryjkov, A. How important is biomass burning in Canada to mercury contamination? *Atmos. Chem. Phys.* **18**, 7263-7286 (2018).
80. Durnford, D. *et al.* How relevant is the deposition of mercury onto snowpacks? – Part 2: A modeling study. *Atmos. Chem. Phys.* **12**, 9251-9274 (2012).
81. Christensen, J. H., Brandt, J., Frohn, L. M. & Skov, H. Modelling of Mercury in the Arctic with the Danish Eulerian Hemispheric Model. *Atmos. Chem. Phys.* **4**, 2251-2257 (2004).
82. Skov, H. *et al.* Variability in gaseous elemental mercury at Villum Research Station, Station Nord, in North Greenland from 1999 to 2017. *Atmos. Chem. Phys.* **20**, 13253-13265 (2020).
83. Cole, A. S. *et al.* Ten-year trends of atmospheric mercury in the high Arctic compared to Canadian sub-Arctic and mid-latitude sites. *Atmos. Chem. Phys.* **13**, 1535-1545 (2013).
84. Gay, D. A. *et al.* The Atmospheric Mercury Network: measurement and initial examination of an ongoing atmospheric mercury record across North America. *Atmos. Chem. Phys.* **13**, 11339-11349 (2013).
85. Tørseth, K. *et al.* Introduction to the European Monitoring and Evaluation Programme (EMEP) and observed atmospheric composition change during 1972–2009. *Atmos. Chem. Phys.* **12**, 5447-5481 (2012).
86. Steffen, A. *et al.* A synthesis of atmospheric mercury depletion event chemistry in the atmosphere and snow. *Atmos. Chem. Phys.* **8**, 1445-1482 (2008).
87. Steffen, A. *et al.* Atmospheric mercury speciation and mercury in snow over time at Alert, Canada. *Atmos. Chem. Phys.* **14**, 2219-2231 (2014).
88. Toyota, K., Dastoor, A. P. & Ryzhkov, A. Air–snowpack exchange of bromine, ozone and mercury in the springtime Arctic simulated by the 1-D model PHANTAS – Part 2: Mercury and its speciation. *Atmos. Chem. Phys.* **14**, 4135-4167 (2014).
89. Sanei, H. *et al.* Wet deposition mercury fluxes in the Canadian sub-Arctic and southern Alberta, measured using an automated precipitation collector adapted to cold regions. *Atmos. Environ.* **44**, 1672-1681 (2010).
90. Sprovieri, F. *et al.* Five-year records of mercury wet deposition flux at GMOS sites in the Northern and Southern hemispheres. *Atmos. Chem. Phys.* **17**, 2689-2708 (2017).
91. Zhou, H., Zhou, C., Hopke, P. K. & Holsen, T. M. Mercury wet deposition and speciated mercury air concentrations at rural and urban sites across New York state: Temporal patterns, sources and scavenging coefficients. *Sci. Total Environ.* **637-638**, 943-953 (2018).
92. Qin, C., Wang, Y., Peng, Y. & Wang, D. Four-year record of mercury wet deposition in one typical industrial city in southwest China. *Atmos. Environ.* **142**, 442-451 (2016).
93. Douglas, T. A. & Blum, J. D. Mercury Isotopes Reveal Atmospheric Gaseous Mercury Deposition Directly to the Arctic Coastal Snowpack. *Environ. Sci. Technol. Lett.* **6**, 235-242 (2019).
94. Yang, Y., Liu, J. & Wang, Z. Reaction mechanisms and chemical kinetics of mercury transformation during coal combustion. *Prog. Energy Combust. Sci.* **79**, 100844 (2020).
95. Galloway, J. N. & Likens, G. E. The collection of precipitation for chemical analysis. *Tellus* **30**, 71-82 (1978).
96. Pearson, C., Howard, D., Moore, C. & Obrist, D. Mercury and trace metal wet deposition across five stations in Alaska: controlling factors, spatial patterns, and source regions. *Atmos. Chem. Phys.* **19**, 6913-6929 (2019).
97. Kochendorfer, J. *et al.* Testing and development of transfer functions for weighing precipitation gauges in WMO-SPICE. *Hydrol. Earth Syst. Sci.* **22**, 1437-1452 (2018).
98. Rasmussen, R. *et al.* How Well Are We Measuring Snow: The NOAA/FAA/NCAR Winter Precipitation Test Bed. *Bull. Ameri. Meteorol. Soc.* **93**, 811-829 (2012).
99. Yang, D., Goodison, B. E., Ishida, S. & Benson, C. S. Adjustment of daily precipitation data at 10 climate stations in Alaska: Application of World Meteorological Organization intercomparison results. *Water Resour. Res.* **34**, 241-256 (1998).

100. Yang, D. An improved precipitation climatology for the Arctic Ocean. *Geophys. Res. Lett.* **26**, 1625-1628 (1999).
101. Wang, X., Bao, Z., Lin, C.-J., Yuan, W. & Feng, X. Assessment of Global Mercury Deposition through Litterfall. *Environ. Sci. Technol.* **50**, 8548-8557 (2016).
102. Kirk, J. L. *et al.* Climate Change and Mercury Accumulation in Canadian High and Subarctic Lakes. *Environ. Sci. Technol.* **45**, 964-970 (2011).
103. Lehnherr, I. *et al.* The world's largest High Arctic lake responds rapidly to climate warming. *Nature Commun.* **9**, 1290 (2018).
104. Muir, D. C. G. *et al.* Spatial Trends and Historical Deposition of Mercury in Eastern and Northern Canada Inferred from Lake Sediment Cores. *Environ. Sci. Technol.* **43**, 4802-4809 (2009).
105. Korosi, J. B. *et al.* Long-term changes in organic matter and mercury transport to lakes in the sporadic discontinuous permafrost zone related to peat subsidence. *Limnol. Oceanogr.* **60**, 1550-1561 (2015).
106. Douglas, T. A. *et al.* A Pulse of Mercury and Major Ions in Snowmelt Runoff from a Small Arctic Alaska Watershed. *Environ. Sci. Technol.* **15**, 11145-11155 (2017).
107. Dommergue, A. *et al.* Deposition of Mercury Species in the Ny-Ålesund Area (79°N) and Their Transfer during Snowmelt. *Environ. Sci. Technol.* **44**, 901-907 (2010).
108. Steffen, A. *et al.* Atmospheric mercury over sea ice during the OASIS-2009 campaign. *Atmos. Chem. Phys.* **13**, 7007-7021 (2013).
109. Andersson, M. E., Sommar, J., Gårdfeldt, K. & Lindqvist, O. Enhanced concentrations of dissolved gaseous mercury in the surface waters of the Arctic Ocean. *Mar. Chem.* **110**, 190-194 (2008).
110. Kalinchuk, V. V., Lopatnikov, E. A., Astakhov, A. S., Ivanov, M. V. & Hu, L. Distribution of atmospheric gaseous elemental mercury (Hg(0)) from the Sea of Japan to the Arctic, and Hg(0) evasion fluxes in the Eastern Arctic Seas: Results from a joint Russian-Chinese cruise in fall 2018. *Sci. Total Environ.* **753**, 142003 (2021).
111. Berg, T., Pfaffhuber, K. A., Cole, A. S., Engelsen, O. & Steffen, A. Ten-year trends in atmospheric mercury concentrations, meteorological effects and climate variables at Zeppelin, Ny-Ålesund. *Atmos. Chem. Phys.* **13**, 6575-6586 (2013).
112. Wang, X. *et al.* Underestimated Sink of Atmospheric Mercury in a Deglaciated Forest Chronosequence. *Environ. Sci. Technol.* **54**, 8083-8093 (2020).
113. Overland, J. E. Less climatic resilience in the Arctic. *Weather Clim. Extremes* **30**, 100275 (2020).
114. Bougoudis, I. *et al.* Long-term time series of Arctic tropospheric BrO derived from UV–VIS satellite remote sensing and its relation to first-year sea ice. *Atmos. Chem. Phys.* **20**, 11869-11892 (2020).
115. Goodsite, M. E., Plane, J. M. C. & Skov, H. A Theoretical Study of the Oxidation of Hg0 to HgBr2 in the Troposphere. *Environ. Sci. Technol.* **38**, 1772-1776 (2004).
116. Goodsite, M. E., Plane, J. M. C. & Skov, H. Correction to A Theoretical Study of the Oxidation of Hg0 to HgBr2 in the Troposphere. *Environ. Sci. Technol.* **46**, 5262-5262 (2012).
117. Shah, V. *et al.* Improved Mechanistic Model of the Atmospheric Redox Chemistry of Mercury. *Environ. Sci. Technol.* (2021).
118. Moore, C. W. *et al.* Convective forcing of mercury and ozone in the Arctic boundary layer induced by leads in sea ice. *Nature* **506**, 81-84 (2014).
119. Douglas, T. A. *et al.* Elevated mercury measured in snow and frost flowers near Arctic sea ice leads. *Geophys. Res. Lett.* **32** (2005).
120. Gleason, J. D. *et al.* Sources and cycling of mercury in the paleo Arctic Ocean from Hg stable isotope variations in Eocene and Quaternary sediments. *Geochim. Cosmochim. Acta* **197**, 245-262 (2017).
121. Masbou, J. *et al.* Hg-Stable Isotope Variations in Marine Top Predators of the Western Arctic Ocean. *ACS Earth Space Chem.* **2**, 479-490 (2018).

122. Olson, C. L., Jiskra, M., Sonke, J. E. & Obrist, D. Mercury in tundra vegetation of Alaska: Spatial and temporal dynamics and stable isotope patterns. *Sci. Total Environ.* **660**, 1502-1512 (2019).
123. Zhou, J. & Obrist, D. Global Mercury Assimilation by Vegetation. *Environ. Sci. Technol.*, In Press (2021).
124. St. Pierre, K. A. *et al.* Importance of Open Marine Waters to the Enrichment of Total Mercury and Monomethylmercury in Lichens in the Canadian High Arctic. *Environ. Sci. Technol.* **49**, 5930-5938 (2015).
125. Landers, D. H. *et al.* Mercury in vegetation and lake sediments from the US Arctic. *Water Air and Soil Pollution* **80**, 591-601 (1995).
126. Drbal, K., Elster, J. & Komarek, J. Heavy metals in water, ice and biological material from Spitsbergen, Svalbard. *Polar Res.* **11**, 99-101 (1992).
127. Wohlgemuth, L. *et al.* A bottom-up quantification of foliar mercury uptake fluxes across Europe. *Biogeosciences* **17**, 6441-6456 (2020).
128. Schuster, P. F. *et al.* Permafrost Stores a Globally Significant Amount of Mercury. *Geophys. Res. Lett.* **45**, 1463-1471 (2018).
129. Lim, A. G. *et al.* A revised northern soil Hg pool, based on western Siberia permafrost peat Hg and carbon observations. *Biogeosciences* **17**, 3083-3097 (2020).
130. Olson, C., Jiskra, M., Biester, H., Chow, J. & Obrist, D. Mercury in Active-Layer Tundra Soils of Alaska: Concentrations, Pools, Origins, and Spatial Distribution. *Global Bigeochem. Cycles* **32**, 1058-1073 (2018).
131. Halbach, K., Mikkelsen, Ø., Berg, T. & Steinnes, E. The presence of mercury and other trace metals in surface soils in the Norwegian Arctic. *Chemosphere* **188**, 567-574 (2017).
132. Hugelius, G. *et al.* Estimated stocks of circumpolar permafrost carbon with quantified uncertainty ranges and identified data gaps. *Biogeosciences* **11**, 6573-6593 (2014).
133. Durnford, D. & Dastoor, A. The behavior of mercury in the cryosphere: A review of what we know from observations. *J. Geophys. Res.: Atmos.* **116** (2011).
134. Hoyer, M., Burke, J. & Keeler, G. Atmospheric sources, transport and deposition of mercury in Michigan: Two years of event precipitation. *Water Air Soil Pollut.* **80**, 199-208 (1995).
135. Keeler, G. J., Gratz, L. E. & Al-wali, K. Long-term Atmospheric Mercury Wet Deposition at Underhill, Vermont. *Ecotoxicology* **14**, 71-83 (2005).
136. Nelson, S. J. *et al.* A comparison of winter mercury accumulation at forested and no-canopy sites measured with different snow sampling techniques. *Appl. Geochem.* **23**, 384-398 (2008).
137. Kurz, A. Y., Blum, J. D., Johnson, M. W., Nadelhoffer, K. & Zak, D. R. Isotopic composition of mercury deposited via snow into mid-latitude ecosystems. *Sci. Total Environ.* **784**, 147252 (2021).
138. Bargagli, R., Agnorelli, C., Borghini, F. & Monaci, F. Enhanced Deposition and Bioaccumulation of Mercury in Antarctic Terrestrial Ecosystems Facing a Coastal Polynya. *Environ. Sci. Technol.* **39**, 8150-8155 (2005).
139. Sherman, L. S., Blum, J. D., Douglas, T. A. & Steffen, A. Frost flowers growing in the Arctic ocean-atmosphere–sea ice–snow interface: 2. Mercury exchange between the atmosphere, snow, and frost flowers. *J. Geophys. Res.: Atmos.* **117**, D00R10 (2012).
140. Douglas, T. A. *et al.* Influence of Snow and Ice Crystal Formation and Accumulation on Mercury Deposition to the Arctic. *Environ. Sci. Technol.* **42**, 1542-1551 (2008).
141. Domine, F. *et al.* The specific surface area and chemical composition of diamond dust near Barrow, Alaska. *J. Geophys. Res.: Atmos.* **116**, D00R06 (2011).
142. Xu, W., Tenuta, M. & Wang, F. Bromide and chloride distribution across the snow-sea ice-ocean interface: A comparative study between an Arctic coastal marine site and an experimental sea ice mesocosm. *J. Geophys. Res.: Oceans* **121**, 5535-5548 (2016).
143. Lalonde, J. D., Poulain, A. J. & Amyot, M. The Role of Mercury Redox Reactions in Snow on Snow-to-Air Mercury Transfer. *Environ. Sci. Technol.* **36**, 174-178 (2002).

144. Poulain, A. J. *et al.* Redox transformations of mercury in an Arctic snowpack at springtime. *Atmos. Environ.* **38**, 6763-6774 (2004).
145. Dommergue, A. *et al.* The fate of mercury species in a sub-arctic snowpack during snowmelt. *Geophys. Res. Lett.* **30**, 1621 (2003).
146. St. Louis, V. L. *et al.* Some sources and sinks of monomethyl and inorganic mercury on Ellesmere island in the Canadian high arctic. *Environ. Sci. Technol.* **39**, 2686-2701 (2005).
147. Faïn, X. *et al.* Mercury in the snow and firn at Summit Station, Central Greenland, and implications for the study of past atmospheric mercury levels. *Atmos. Chem. Phys.* **8**, 3441-3457 (2008).
148. Ferrari, C. P. *et al.* Snow-to-air exchanges of mercury in an Arctic seasonal snow pack in Ny-Ålesund, Svalbard. *Atmos. Environ.* **39**, 7633-7645 (2005).
149. Johnson, K. P., Blum, J. D., Keeler, G. J. & Douglas, T. A. Investigation of the deposition and emission of mercury in arctic snow during an atmospheric mercury depletion event. *J. Geophys. Res.: Atmos.* **113** (2008).
150. Kamp, J., Skov, H., Jensen, B. & Sørensen, L. L. Fluxes of gaseous elemental mercury (GEM) in the High Arctic during atmospheric mercury depletion events (AMDEs). *Atmos. Chem. Phys.* **18**, 6923-6938 (2018).
151. Mann, E. A. *et al.* Photoreducible Mercury Loss from Arctic Snow Is Influenced by Temperature and Snow Age. *Environ. Sci. Technol.* **49**, 12120-12126 (2015).
152. Boutron, C. F., Vandal, G. M., Fitzgerald, W. F. & Ferrari, C. P. A forty year record of Mercury in central Greenland snow. *Geophys. Res. Lett.* **25**, 3315-3318 (1998).
153. Brooks, S. *et al.* Temperature and sunlight controls of mercury oxidation and deposition atop the Greenland ice sheet. *Atmos. Chem. Phys.* **11**, 8295-8306 (2011).
154. Zheng, J. Archives of total mercury reconstructed with ice and snow from Greenland and the Canadian High Arctic. *Sci. Total Environ.* **509-510**, 133-144 (2015).
155. Farinotti, D. *et al.* A consensus estimate for the ice thickness distribution of all glaciers on Earth. *Nat. Geosci.* **12**, 168-173 (2019).
156. Forsberg, R., Sørensen, L. & Simonsen, S. in *Integrative Study of the Mean Sea Level and Its Components* (eds Anny Cazenave, Nicolas Champollion, Frank Paul, & Jérôme Benveniste) 91-106 (Springer International Publishing, 2017).
157. Ciracì, E., Velicogna, I. & Swenson, S. Continuity of the Mass Loss of the World's Glaciers and Ice Caps From the GRACE and GRACE Follow-On Missions. *Geophys. Res. Lett.* **47**, e2019GL086926 (2020).
158. Hawkings, J. R. *et al.* Large subglacial source of mercury from the southwestern margin of the Greenland Ice Sheet. *Nat. Geosci.* **14**, 496-502 (2021).
159. Friske, P. W. B. *et al.* (ed Geological Survey of Canada) (1994).
160. Halm, D. R. & Dornblaser, M. M. Water and Sediment Quality in the Yukon River and its Tributaries Between Atlin, British Columbia, Canada, and Eagle, Alaska, USA, 2004. Report No. 2007-1197, (2007).
161. Nagorski, S. A., Vermilyea, A. W. & Lamborg, C. H. Mercury export from glacierized Alaskan watersheds as influenced by bedrock geology, watershed processes, and atmospheric deposition. *Geochim. Cosmochim. Acta* **304**, 32-49 (2021).
162. Søndergaard, J., Riget, F., Tamstorf, M. P. & Larsen, M. M. Mercury Transport in a Low-Arctic River in Kobbefjord, West Greenland (64A degrees N). *Water Air Soil Pollut.* **223**, 4333-4342 (2012).
163. Overeem, I. *et al.* Substantial export of suspended sediment to the global oceans from glacial erosion in Greenland. *Nat. Geosci.* **10**, 859–863 (2017).
164. Pfeffer, W. T. *et al.* The Randolph Glacier Inventory: a globally complete inventory of glaciers. *J. Glaciol.* **60**, 537-552 (2014).
165. Zolkos, S. *et al.* Mercury Export from Arctic Great Rivers. *Environ. Sci. Technol.* **54**, 4140-4148 (2020).

166. Leitch, D. R. *et al.* The delivery of mercury to the Beaufort Sea of the Arctic Ocean by the Mackenzie River. *Sci. Total Environ.* **373**, 178-195 (2007).
167. Lim, A. G. *et al.* Enhanced particulate Hg export at the permafrost boundary, western Siberia. *Environ. Pollut.* **254**, 113083 (2019).
168. Schuster, P. F. *et al.* Mercury Export from the Yukon River Basin and Potential Response to a Changing Climate. *Environ. Sci. Technol.* **45**, 9262-9267 (2011).
169. Emmerton, C. A. *et al.* Mercury Export to the Arctic Ocean from the Mackenzie River, Canada. *Environ. Sci. Technol.* **47**, 7644-7654 (2013).
170. Walvoord, M. A. & Striegl, R. G. Increased groundwater to stream discharge from permafrost thawing in the Yukon River basin: Potential impacts on lateral export of carbon and nitrogen. *Geophys. Res. Lett.* **34**, L12402 (2007).
171. Vonk, J. E. *et al.* Reviews and syntheses: Effects of permafrost thaw on Arctic aquatic ecosystems. *Biogeosciences* **12**, 7129-7167 (2015).
172. Tank, S. E. *et al.* Landscape matters: Predicting the biogeochemical effects of permafrost thaw on aquatic networks with a state factor approach. *Permafrost Periglacial Processes* **31**, 358-370 (2020).
173. Sukhenko, S. A., Papina, T. S. & Pozdnjakov, S. R. Transport of mercury by the Katun river, West Siberia. *Hydrobiologia* **228**, 23-28 (1992).
174. Fedorov, Y. A. *et al.* Patterns of mercury distribution in bottom sediments along the Severnaya Dvina-White Sea section. *Dokl. Earth Sci.* **436**, 51-54 (2011).
175. Bliss, A., Hock, R. & Radić, V. Global response of glacier runoff to twenty-first century climate change. *J. Geophys. Res.: Earth Surf.* **119**, 717-730 (2014).
176. Delaney, I. & Adhikari, S. Increased Subglacial Sediment Discharge in a Warming Climate: Consideration of Ice Dynamics, Glacial Erosion, and Fluvial Sediment Transport. *Geophys. Res. Lett.* **47**, e2019GL085672 (2020).
177. van Pelt, W. J. J., Schuler, T. V., Pohjola, V. A. & Pettersson, R. Accelerating future mass loss of Svalbard glaciers from a multi-model ensemble. *J. Glaciol.* **67**, 485-499 (2021).
178. Muntjewerf, L. *et al.* Accelerated Greenland Ice Sheet Mass Loss Under High Greenhouse Gas Forcing as Simulated by the Coupled CESM2.1-CISM2.1. *J. Adv. Model. Earth Syst.* **12**, e2019MS002031 (2020).
179. Mu, C. *et al.* Carbon and mercury export from the Arctic rivers and response to permafrost degradation. *Water Res.* **161**, 54-60 (2019).
180. Overduin, P. P. *et al.* Coastal changes in the Arctic. *Geological Society, London, Special Publications* **388**, 103 (2014).
181. Gibbs, A. E., Ohman, K. A. & Richmond, B. M. (ed United States Geological Survey) (2015).
182. Couture, N. J., Irrgang, A., Pollard, W., Lantuit, H. & Fritz, M. Coastal Erosion of Permafrost Soils Along the Yukon Coastal Plain and Fluxes of Organic Carbon to the Canadian Beaufort Sea. *J. Geophys. Res.: Biogeosci.* **123**, 406-422 (2018).
183. Leitch, D. R. *Mercury Distribution in Water and Permafrost of the Lower Mackenzie Basin, Their Contribution to the Mercury Contamination in the Beaufort Sea Marine Ecosystem, and Potential Effects of Climate Variation* Master of Science thesis, University of Manitoba, (2006).
184. Outridge, P. M. & Sanei, H. Does organic matter degradation affect the reconstruction of pre-industrial atmospheric mercury deposition rates from peat cores? — A test of the hypothesis using a permafrost peat deposit in northern Canada. *Int. J. Coal Geol.* **83**, 73-81 (2010).
185. Lantuit, H. *et al.* The Arctic Coastal Dynamics Database: A New Classification Scheme and Statistics on Arctic Permafrost Coastlines. *Estuaries Coasts* **35**, 383-400 (2012).
186. Irrgang, A. M. *et al.* Variability in Rates of Coastal Change Along the Yukon Coast, 1951 to 2015. *J. Geophys. Res.: Earth Surf.* **123**, 779-800 (2018).
187. Wang, F., Macdonald, R. W., Armstrong, D. A. & Stern, G. A. Total and Methylated Mercury in the Beaufort Sea: The Role of Local and Recent Organic Remineralization. *Environ. Sci. Technol.* **46**, 11821-11828 (2012).

188. Lehnherr, I., St Louis, V. L., Hintelmann, H. & Kirk, J. L. Methylation of inorganic mercury in polar marine waters. *Nat. Geosci.* **4**, 298-302 (2011).
189. Kirk, J. L. *et al.* Methylated Mercury Species in Marine Waters of the Canadian High and Sub Arctic. *Environ. Sci. Technol.* **42**, 8367-8373 (2008).
190. St. Louis, V. L. *et al.* Methylated Mercury Species in Canadian High Arctic Marine Surface Waters and Snowpacks. *Environ. Sci. Technol.* **41**, 6433-6441 (2007).
191. Tesán Onrubia, J. A. *et al.* Mercury Export Flux in the Arctic Ocean Estimated from 234Th/238U Disequilibria. *ACS Earth Space Chem.* **4**, 795-801 (2020).
192. Heimbürger, L.-E. *et al.* Shallow methylmercury production in the marginal sea ice zone of the central Arctic Ocean. *Sci. Rep.* **5**, 10318 (2015).
193. Cossa, D. *et al.* Mercury distribution and transport in the North Atlantic Ocean along the GEOTRACES-GA01 transect. *Biogeosciences* **15**, 2309-2323 (2018).
194. Charette, M. A. *et al.* The Transpolar Drift as a Source of Riverine and Shelf-Derived Trace Elements to the Central Arctic Ocean. *J. Geophys. Res.: Oceans* **125**, e2019JC015920 (2020).
195. Bowman, K. L., Lamborg, C. H. & Agather, A. M. A global perspective on mercury cycling in the ocean. *Sci. Total Environ.* **710**, 136166 (2020).
196. Kim, H. *et al.* Contrasting distributions of dissolved gaseous mercury concentration and evasion in the North Pacific Subarctic Gyre and the Subarctic Front. *Deep Sea Res. Part I* **110**, 90-98 (2016).
197. Outridge, P. M., Macdonald, R. W., Wang, F., Stern, G. A. & Dastoor, A. P. A mass balance inventory of mercury in the Arctic Ocean. *Environ. Chem.* **5**, 89-111 (2008).
198. Parkinson, C. L. & Cavalieri, D. J. Arctic sea ice variability and trends, 1979–2006. *J. Geophys. Res.: Oceans* **113**, C07003 (2008).
199. Cavalieri, D. J. & Parkinson, C. L. Arctic sea ice variability and trends, 1979-2010. *Cryosphere* **6**, 881-889 (2012).
200. Arrigo, K. R. & van Dijken, G. L. Continued increases in Arctic Ocean primary production. *Prog. Oceanogr.* **136**, 60-70 (2015).
201. Hu, H. *et al.* Mercury Reduction and Cell-Surface Adsorption by Geobacter sulfurreducens PCA. *Environ. Sci. Technol.* **47**, 10922-10930 (2013).
202. Møller, A. K. *et al.* Mercuric reductase genes (merA) and mercury resistance plasmids in High Arctic snow, freshwater and sea-ice brine. *FEMS Microbiol. Ecol.* **87**, 52-63 (2014).
203. Whalin, L., Kim, E.-H. & Mason, R. Factors influencing the oxidation, reduction, methylation and demethylation of mercury species in coastal waters. *Mar. Chem.* **107**, 278-294 (2007).
204. Zhang, Y., Soerensen, A. L., Schartup, A. T. & Sunderland, E. M. A Global Model for Methylmercury Formation and Uptake at the Base of Marine Food Webs. *Global Bigeochem. Cycles* **34**, e2019GB006348 (2020).
205. Chaulk, A., Stern, G. A., Armstrong, D., Barber, D. G. & Wang, F. Mercury Distribution and Transport Across the Ocean−Sea-Ice−Atmosphere Interface in the Arctic Ocean. *Environ. Sci. Technol.* **45**, 1866-1872 (2011).
206. Beattie, S. A. *et al.* Total and Methylated Mercury in Arctic Multiyear Sea Ice. *Environ. Sci. Technol.* **48**, 5575-5582 (2014).
207. Klunder, M. B. *et al.* Dissolved iron in the Arctic shelf seas and surface waters of the central Arctic Ocean: Impact of Arctic river water and ice-melt. *J. Geophys. Res.: Oceans* **117**, C01027 (2012).
208. Cossa, D. *et al.* Mercury in the Southern Ocean. *Geochim. Cosmochim. Acta* **75**, 4037-4052 (2011).
209. Wang, F., Pućko, M. & Stern, G. Transport and transformation of contaminants in sea ice. *Sea Ice*, 472-491 (2017).
210. Tsubouchi, T. *et al.* The Arctic Ocean Seasonal Cycles of Heat and Freshwater Fluxes: Observation-Based Inverse Estimates. *J. Phys. Oceanogr.* **48**, 2029-2055 (2018).

211. Østerhus, S. *et al.* Arctic Mediterranean exchanges: a consistent volume budget and trends in transports from two decades of observations. *Ocean Sci.* **15**, 379-399 (2019).
212. Rachold, V. *et al.* in *The Organic Carbon Cycle in the Arctic Ocean* (eds Ruediger Stein & Robie W. MacDonald) 33-55 (Springer Berlin Heidelberg, 2004).
213. Gamboa, A., Montero-Serrano, J.-C., St-Onge, G., Rochon, A. & Desiage, P.-A. Mineralogical, geochemical, and magnetic signatures of surface sediments from the Canadian Beaufort Shelf and Amundsen Gulf (Canadian Arctic). *Geochem. Geophys. Geosyst.* **18**, 488-512 (2017).
214. Lamborg, C. H., Hammerschmidt, C. R. & Bowman, K. L. An examination of the role of particles in oceanic mercury cycling. *Philos Trans A Math Phys Eng Sci* **374**, 20150297 (2016).
215. Pućko, M. *et al.* Transformation of Mercury at the Bottom of the Arctic Food Web: An Overlooked Puzzle in the Mercury Exposure Narrative. *Environ. Sci. Technol.* **48**, 7280-7288 (2014).
216. Hayes, C. T. *et al.* Global Ocean Sediment Composition and Burial Flux in the Deep Sea. *Global Bigeochem. Cycles* **35**, e2020GB006769 (2021).
217. Aksentov, K. I. *et al.* Assessment of mercury levels in modern sediments of the East Siberian Sea. *Mar. Pollut. Bull.* **168**, 112426 (2021).
218. MacMillan, G. A., Girard, C., Chételat, J., Laurion, I. & Amyot, M. High Methylmercury in Arctic and Subarctic Ponds is Related to Nutrient Levels in the Warming Eastern Canadian Arctic. *Environ. Sci. Technol.* **49**, 7743-7753 (2015).
219. Pelletier, N., Chételat, J., Blarquez, O. & Vermaire, J. C. Paleolimnological Assessment of Wildfire-Derived Atmospheric Deposition of Trace Metal(loid)s and Major Ions to Subarctic Lakes (Northwest Territories, Canada). *J. Geophys. Res.: Biogeosci.* **125**, e2020JG005720 (2020).
220. Ivanov, V. V., Shapiro, G. I., Huthnance, J. M., Aleynik, D. L. & Golovin, P. N. Cascades of dense water around the world ocean. *Prog. Oceanogr.* **60**, 47-98 (2004).
221. Roeske, T., Loeff, M. R. v., Middag, R. & Bakker, K. Deep water circulation and composition in the Arctic Ocean by dissolved barium, aluminium and silicate. *Mar. Chem.* **132-133**, 56-67 (2012).
222. Bianchi, T. S. The role of terrestrially derived organic carbon in the coastal ocean: A changing paradigm and the priming effect. *PNAS* **108**, 19473 (2011).
223. Rontani, J.-F. *et al.* Degradation of sterols and terrigenous organic matter in waters of the Mackenzie Shelf, Canadian Arctic. *Org. Geochem.* **75**, 61-73 (2014).
224. Custodio, D., Ebinghaus, R., Spain, T. G. & Bieser, J. Source apportionment of atmospheric mercury in the remote marine atmosphere: Mace Head GAW station, Irish western coast. *Atmos. Chem. Phys.* **20**, 7929-7939 (2020).
225. Vermilyea, A. W. *et al.* Continuous proxy measurements reveal large mercury fluxes from glacial and forested watersheds in Alaska. *Sci. Total Environ.* **599-600**, 145-155 (2017).
226. Hare, A., Stern, G. A., Macdonald, R. W., Kuzyk, Z. Z. & Wang, F. Contemporary and preindustrial mass budgets of mercury in the Hudson Bay Marine System: The role of sediment recycling. *Sci. Total Environ.* **406**, 190-204 (2008).
227. Kirk, J. L. & St. Louis, V. L. Multiyear Total and Methyl Mercury Exports from Two Major Sub-Arctic Rivers Draining into Hudson Bay, Canada. *Environ. Sci. Technol.* **43**, 2254-2261 (2009).
228. Semkin, R. G., Mierle, G. & Neureuther, R. J. Hydrochemistry and mercury cycling in a High Arctic watershed. *Sci. Total Environ.* **342**, 199-221 (2005).
229. Haine, T. W. N. *et al.* Arctic freshwater export: Status, mechanisms, and prospects. *Global Planet. Change* **125**, 13-35 (2015).
230. Mason, R. P. *et al.* Mercury biogeochemical cycling in the ocean and policy implications. *Environ. Res.* **119**, 101-117 (2012).
231. Bravo, A. G. & Cosio, C. Biotic formation of methylmercury: A bio–physico–chemical conundrum. *Limnol. Oceanogr.* **65**, 1010-1027 (2020).

232. Durnford, D., Dastoor, A., Figuera-Nieto, D. & Ryjkov, A. Long range transport of mercury to the Arctic and across Canada. *Atmos. Chem. Phys.* **10**, 6063-6086 (2010).
233. Burt, A. *et al.* Mercury uptake within an ice algal community during the spring bloom in first-year Arctic sea ice. *J. Geophys. Res.: Oceans* **118**, 4746-4754 (2013).
234. Villar, E., Cabrol, L. & Heimbürger-Boavida, L.-E. Widespread microbial mercury methylation genes in the global ocean. *Environ. Microbiol. Rep.* **12**, 277-287 (2020).
235. Gilmour, C. C. *et al.* Mercury Methylation by Novel Microorganisms from New Environments. *Environ. Sci. Technol.* **47**, 11810-11820 (2013).
236. Lee, C.-S. & Fisher, N. S. Methylmercury uptake by diverse marine phytoplankton. *Limnol. Oceanogr.* **61**, 1626-1639 (2016).
237. Schartup, A. T. *et al.* A Model for Methylmercury Uptake and Trophic Transfer by Marine Plankton. *Environ. Sci. Technol.* **52**, 654-662 (2018).
238. Wu, P. *et al.* The importance of bioconcentration into the pelagic food web base for methylmercury biomagnification: A meta-analysis. *Sci. Total Environ.* **646**, 357-367 (2019).

Figures

Arctic mercury cycling

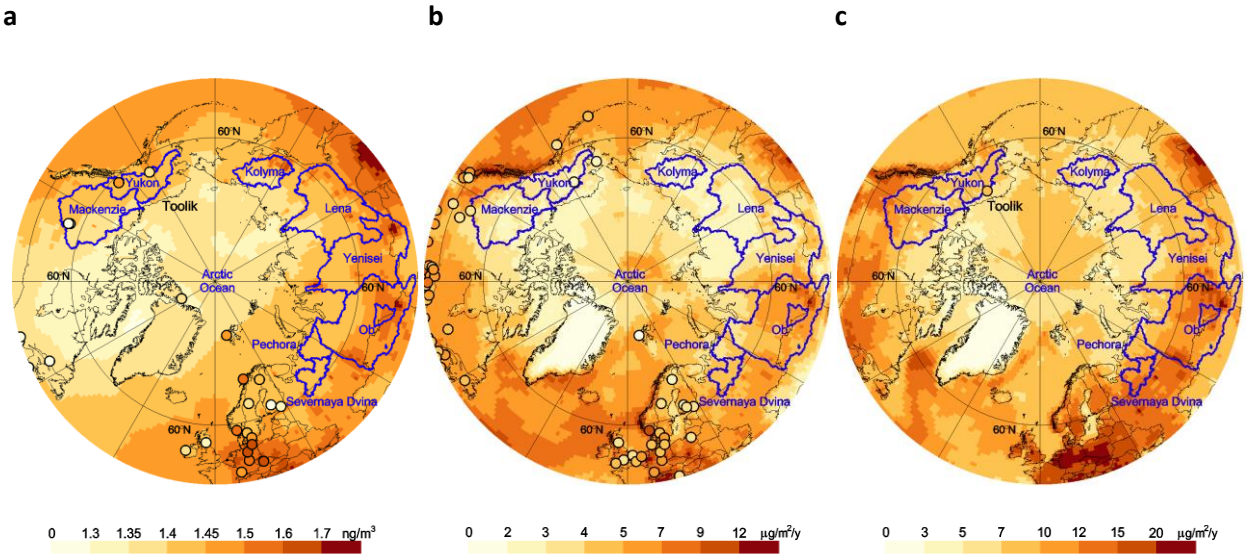

Figure 1. | Atmospheric Hg distribution in the Arctic. a| Model ensemble (DEHM, GEM-MACH-Hg, GLEMOS, GOES-Chem) simulated (this Review) annual average surface air gaseous elemental mercury (Hg(0)) concentrations in 2015. **b**| Annual mercury (Hg) wet deposition flux in 2015. **c**| Annual Hg total deposition in the Arctic in 2015. Circles show observations in the same color scale. The blue lines delineate major pan-Arctic river watersheds. Air concentrations and wet deposition observations are from ECCC-AMM[83], AMNet[84], EMEP[85] and REF[224], and total deposition observation is from REF [29].

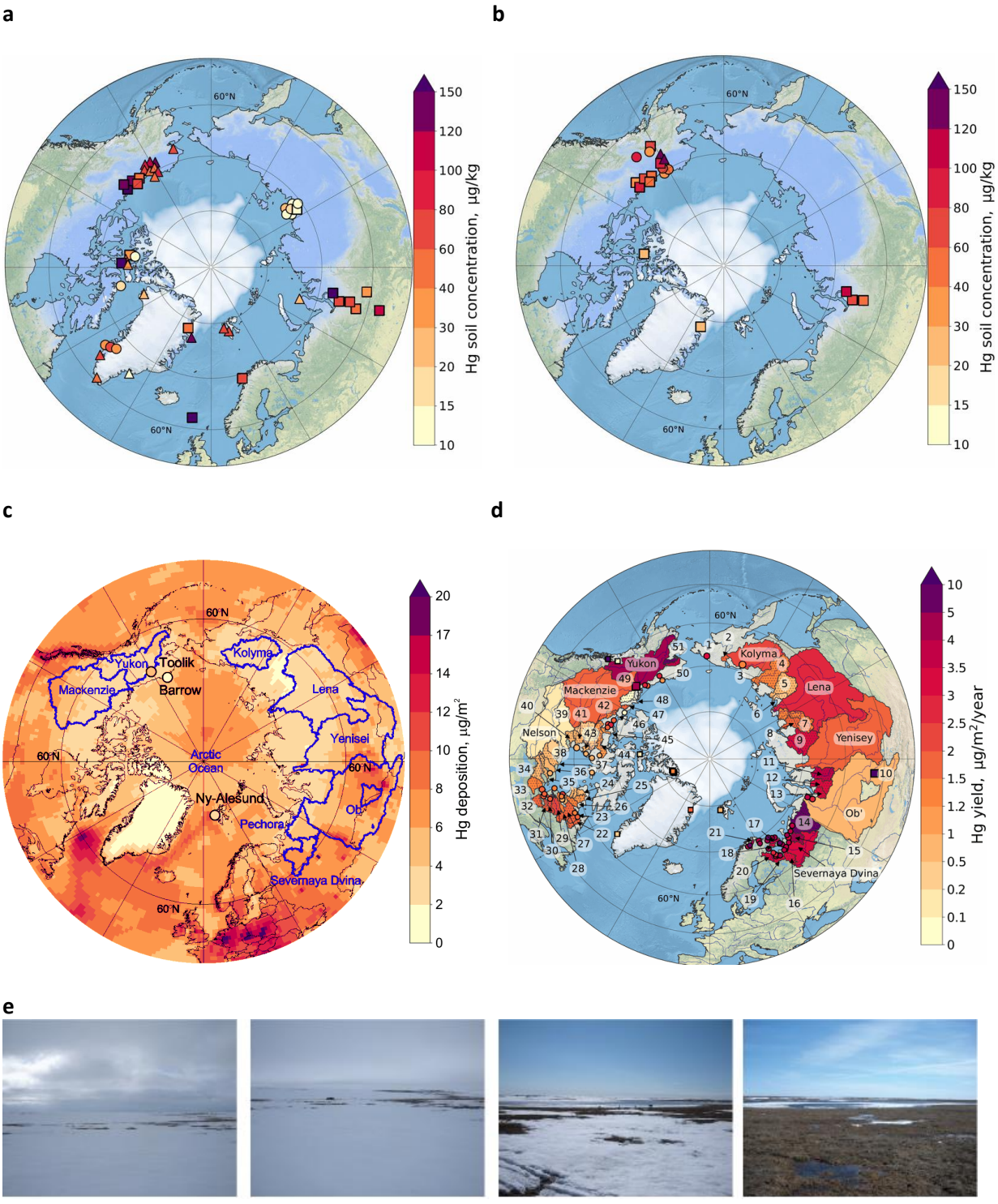

Figure 2. | Distribution of total Hg in Arctic soils, wintertime deposition and rivers. a| Mean mercury (Hg) concentrations of active layer soils within 0-1 m depth. **b|** Mean Hg concentration of permafrost

layer soils within 0-1 m depth. Symbols in Figs. a-b represent the soil type with squares for organic soils, circles for mineral soils and triangles for combined organic/mineral soils **c**| Wintertime (September-May) model ensemble simulated Hg deposition to snowpack. Observations are shown in circles **d**| Annual river total mercury (THg) yields (annual riverine THg mass flux to the Arctic Ocean divided by watershed area) for pan-Arctic watersheds. Larger watersheds (> 10,000 km^2) are delineated where possible, while smaller watersheds are represented by symbols. Solid colored watersheds and squares represent measured THg yields (n=32) reported in REF[7,16-18,107,162,165,169,173,225-228]. Hatched watersheds and circles are THg yields (n=100) modelled in REF[7]. Numbered watersheds are: 1) Amguema, 2) Palyavaam, 3) Bolshoy Anyuy, 4) Indigirka, 5) Yana, 6) Omoloy, 7) Olenek, 8) Anabar, 9) Khatanga, 10) Katun, 11) Taz, 12) Pur, 13) Nadym, 14) Pechora, 15) Mezen, 16) Onega, 17) Ponoy, 18) Varzuga, 19) Nyzhny Vig (Sor), 20) Kem, 21) Tana, 22) George, 23) À la Baleine, 24) Povungnituq, 25) Arnaud, 26) Aux Feuilles, 27) Koksoak, 28) Grande Rivière de la Baleine, 29) La Grande Rivière, 30) Eastmain, 31) Rupert, 32) Nottaway, 33) Moose, 34) Albany, 35) Attawapiskat, 36) Winisk, 37) Severn, 38) Hayes, 39) Churchill, 40) Seal, 41) Thlewiaza, 42) Ferguson, 43) Thelon, 44) Back, 45) Ellice, 46) Coppermine, 47) Hornaday, 48) Anderson, 49) Peel, 50) Noatak, 51) Kobuk. For rivers with multiple yield estimates, only the estimate for the most recent time period is shown. **e**| Repeat images during spring melt in Utqiaġvik (formerly Barrow), Alaska during a typical spring melt. In a matter of a few weeks the tundra surface goes from completely snow covered to a wet vegetation and soil surface exposed to continuous sunlight.

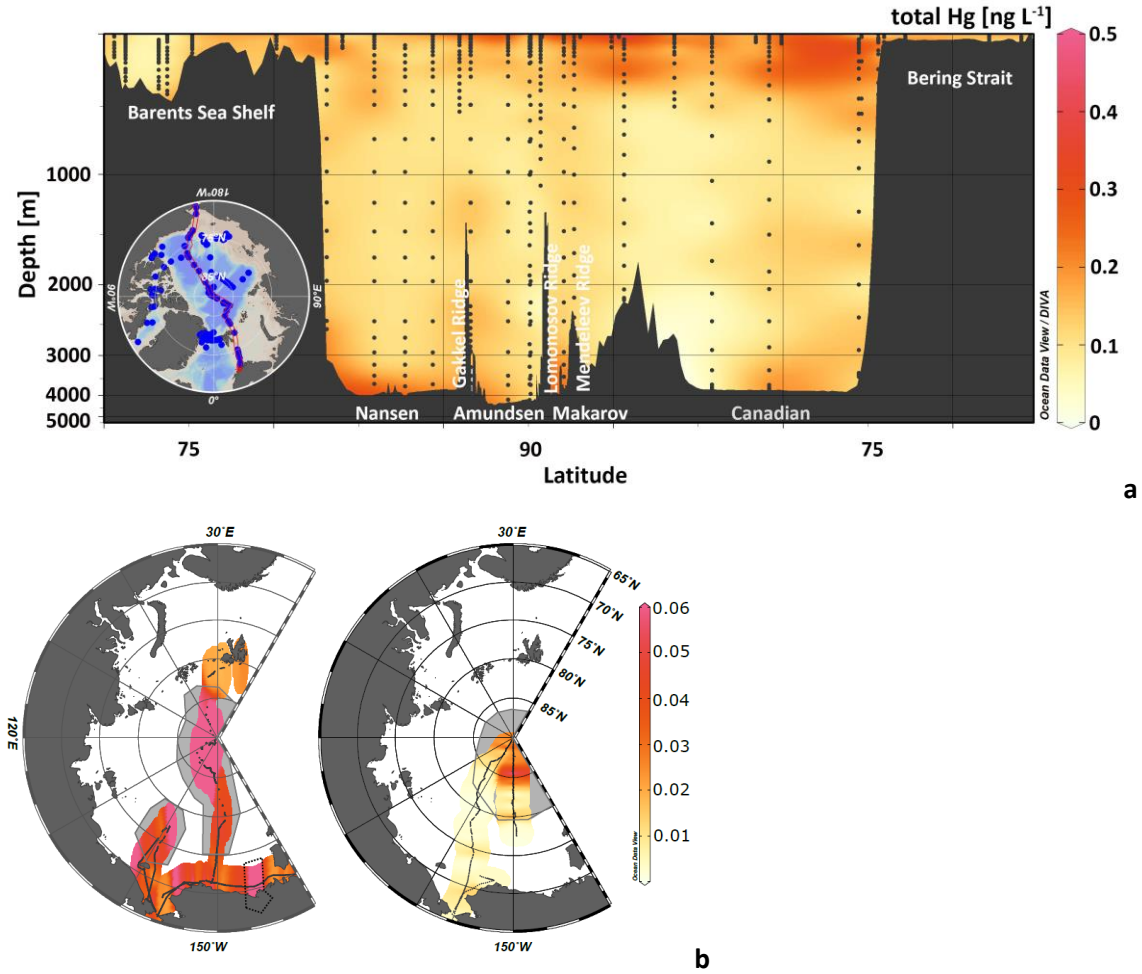

Figure 3. | Spatial distribution of Hg in the Arctic Ocean. **a**| Synoptic pan-Arctic transect of total Hg concentrations during the 2015 GEOTRACES cruises (ng L^{-1})[22,191,194]. The insert map shows the transect (red band) and available Hg observations (blue dots). **b**| Surface water Hg(0) concentrations (ng L^{-1}) in the Arctic Ocean during a summer (left[109]) and fall (right[19]) cruise. Grey areas indicate ice-covered water. The area indicated with a punctuated line represents the outflow region from the Mackenzie River Basin. Ocean currents transport Hg via waters entering the AO from the Atlantic Ocean (235±31.7x10^3 km^3 y^{-1}, Fram Strait; 72.9±38.0x10^3 km^3 y^{-1}, Barents Sea Opening), and the Pacific Ocean (22.2±22.2x10^3 km^3 y^{-1}, Bering Strait), and exiting the AO through the Davis Strait (66.6±22.2x10^3 km^3 y^{-1}) and Fram Strait (273±114x10^3 km^3 y^{-1}) into the Atlantic Ocean[210,229].

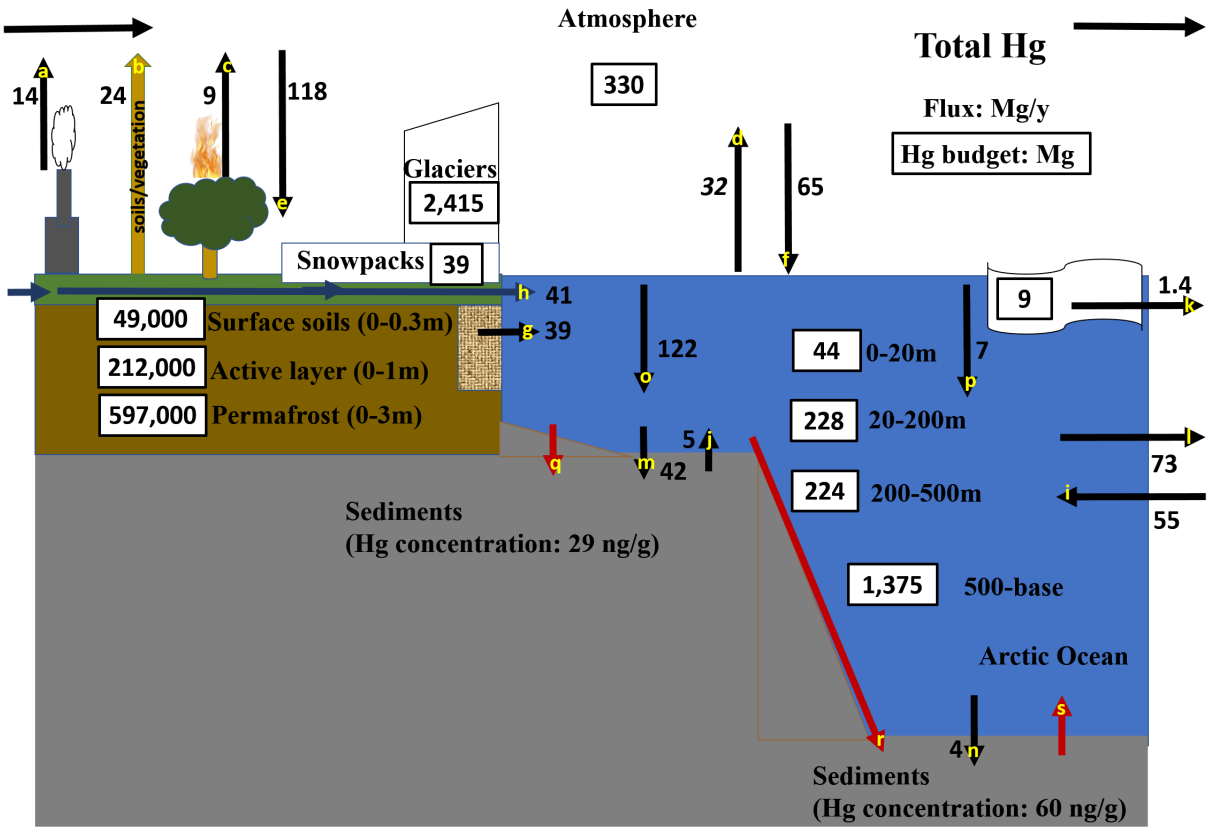

Figure 4 | Arctic Hg inter-compartmental annual fluxes and reservoir budgets. Best estimates (black numbers) and uncertainties in terrestrial and oceanic Hg annual fluxes (identified by arrows with letters) are: anthropogenic (a, 14 Mg y^{-1}), natural and legacy soils/vegetation volatilization (b, $24^{+35.1}_{-17.5}$ Mg y^{-1}), wildfires (c, 8.8±6.4 Mg y^{-1}), and ocean (d, 32^{+13}_{-9} Mg y^{-1}) emissions; terrestrial (e, 118±20 Mg y^{-1}), and ocean (f, 64.5±19.8 Mg) deposition; coastal erosion (g, 39^{+13}_{-21} Mg y^{-1}), river (h, 41±4 Mg y^{-1}), ocean (i, 55+7 Mg y^{-1}), and benthic shelf (j, 5 Mg y^{-1}) imports; sea ice (k, 1.4± 0.4 Mg y^{-1}), ocean (l, 73±8 Mg y^{-1}), shelf burial (m, 42±31 Mg y^{-1}) and deep ocean burial (n, 3.9±0.7 Mg y^{-1}) exports; and in-ocean shelf (o, 122±55 Mg y^{-1}) and deep ocean (p, 7.2±17 Mg y^{-1}) downward fluxes from surface waters. Best estimates (black numbers) and uncertainties for Hg budgets in reservoirs are: atmosphere (330^{+30}_{-40} Mg), glaciers (2,415±22 Mg), snowpacks (39^{+3}_{-4} Mg), soils (surface, 0-0.3 m: 49±23 Gg; active layer, 0-1 m: 212±28 Gg; permafrost, 0-3 m: 597 Gg), and Arctic Ocean (44±22 Mg, 0-20 m; 228±112 Mg, 20-200 m; 224±106 Mg, 200-500 m; 1,375±616 Mg, 500 m and deeper). Red arrows indicate unknown Hg fluxes of burial in estuaries and inner shelf (q), transport from shelf to deep Arctic Ocean basin (r), and benthic deep basin (s) fluxes. Arctic Ocean sediments Hg concentrations are 28.9±22.0 ng g^{-1} in shelf and 60.4±44.5 ng g^{-1} in deep basin. Arctic land is defined as region north of 60° N and the Arctic Ocean is defined as the central basin, and Barents, Kara, Laptev East Siberian, Chukchi and Beaufort Seas (94.5 x 10^5 km^2, total ocean surface area; 53% shelf). The Hg fluxes and budgets were estimated in this Review based on multi-model ensemble simulations and peer-reviewed literature.

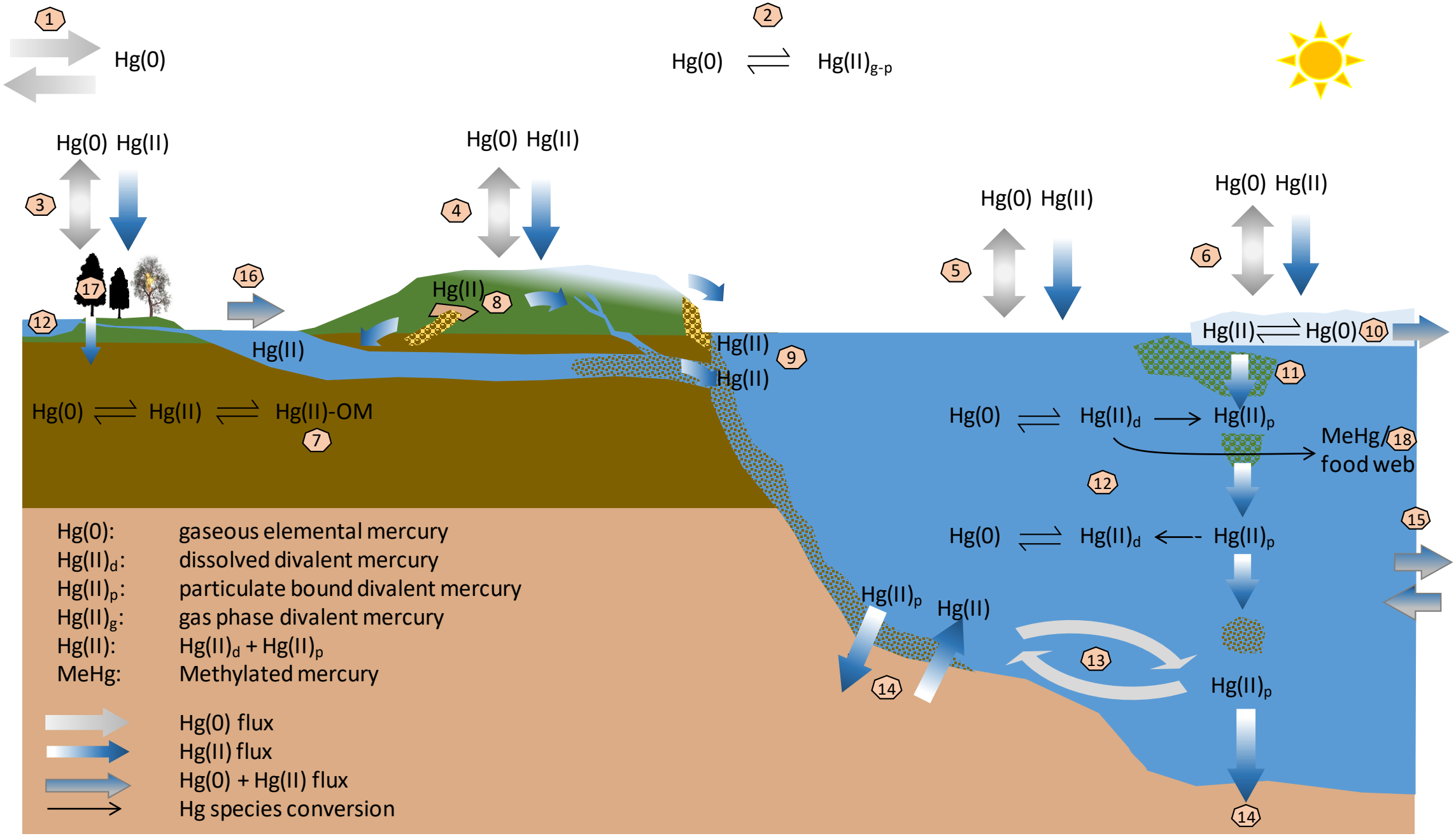
1
Hg(0)
2
Hg(0) ⇌ Hg(II)g-p
Hg(0) Hg(II)
3
Hg(0) Hg(II)
4
Hg(0) Hg(II)
5
Hg(0) Hg(II)
6
17
16
Hg(II)
8
12
Hg(II)
Hg(II)
9
Hg(II)
Hg(II) ⇌ Hg(0)
10
11
Hg(0) ⇌ Hg(II) ⇌ Hg(II)-OM
7
Hg(0) ⇌ Hg(II)d → Hg(II)p
MeHg/
food web
18
12
Hg(0) ⇌ Hg(II)d ← Hg(II)p
15
Hg(II)p
Hg(II)
13
Hg(II)p
14
14
Hg(0): gaseous elemental mercury
Hg(II)d: dissolved divalent mercury
Hg(II)p: particulate bound divalent mercury
Hg(II)g: gas phase divalent mercury
Hg(II): Hg(II)d + Hg(II)p
MeHg: Methylated mercury
Hg(0) flux
Hg(II) flux
Hg(0) + Hg(II) flux
Hg species conversion

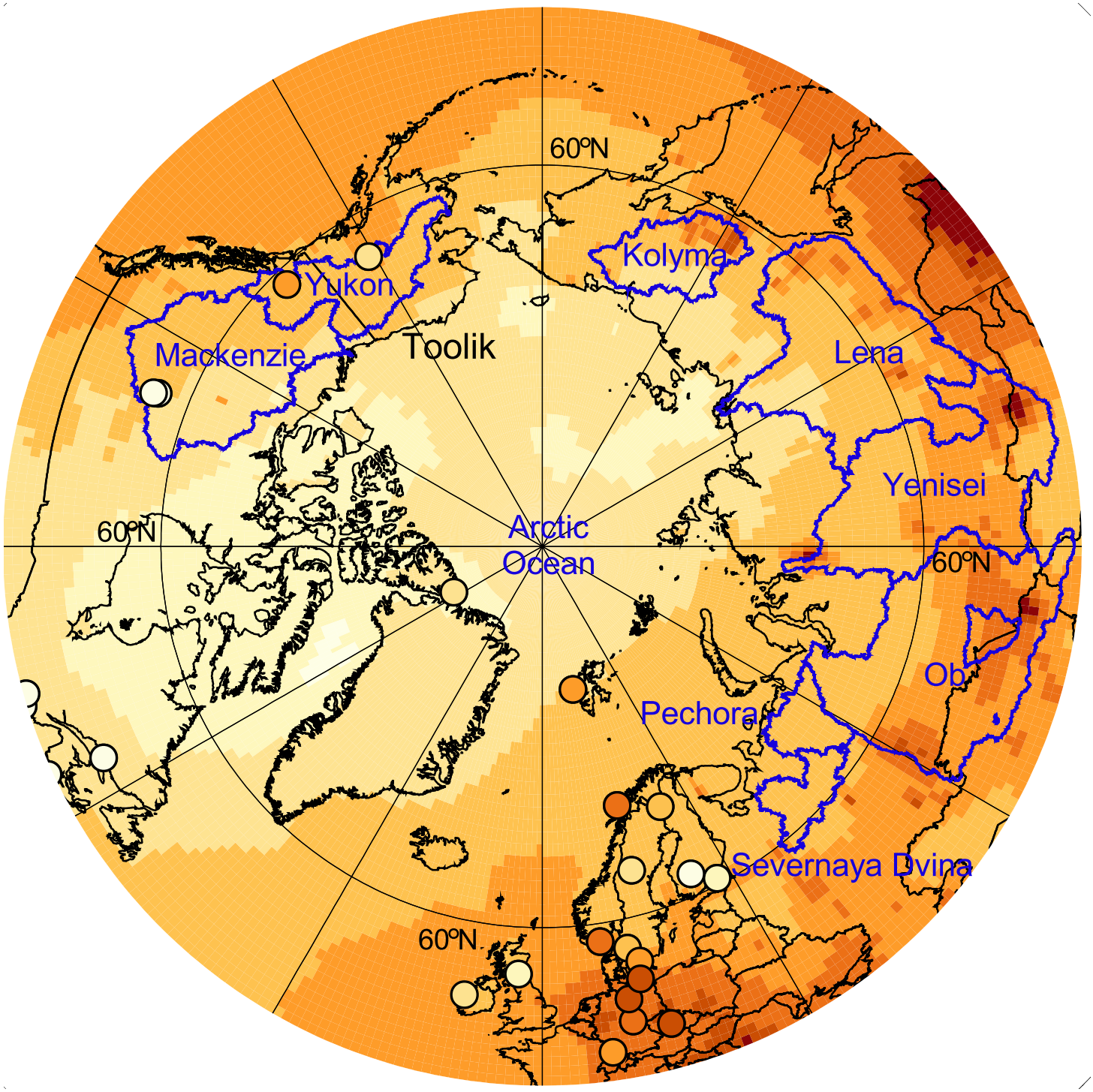
60°N
Kolyma
Yukon
Toolik
Mackenzie
Lena
Yenisei
60°N
Arctic
Ocean
60°N
Ob
Pechora
Severnaya Dvina
60°N

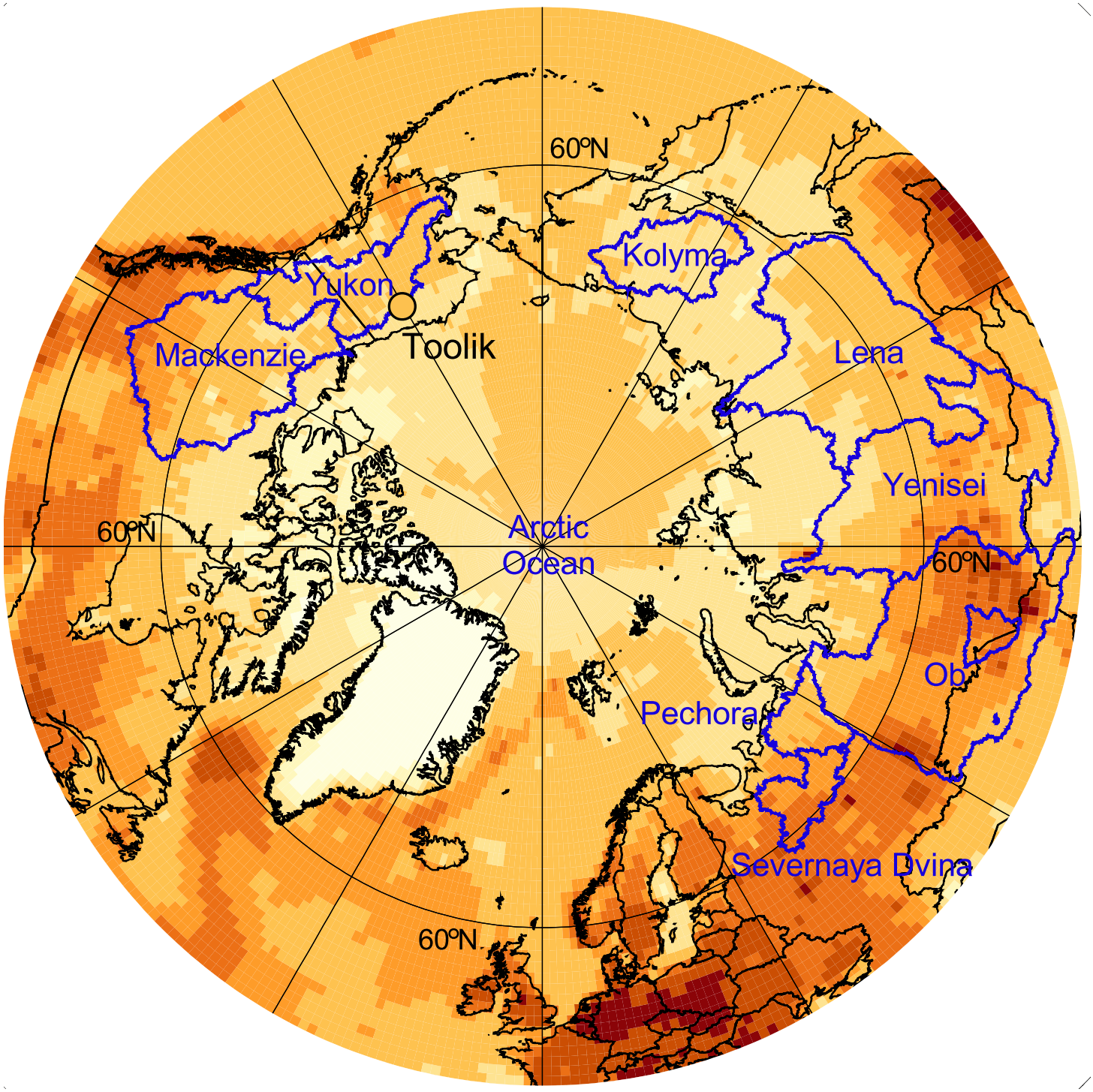
60°N
Kolyma
Yukon
Toolik
Mackenzie
Lena
Yenisei
60°N
Arctic
Ocean
60°N
Ob
Pechora
Severnaya Dvina
60°N

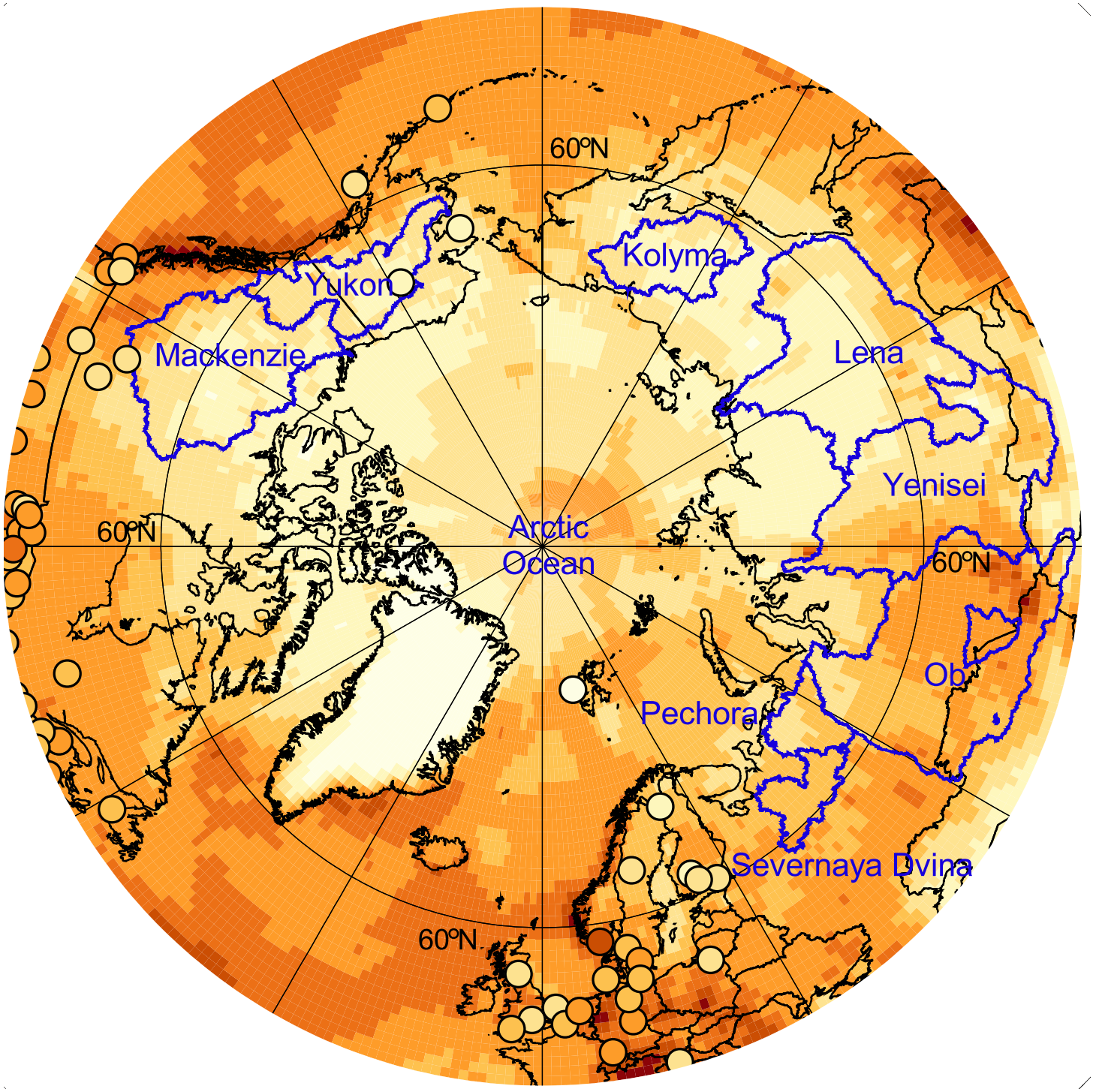
60°N
Kolyma
Yukon
Mackenzie
Lena
Yenisei
60°N
Arctic
Ocean
60°N
Ob
Pechora
Severnaya Dvina
60°N

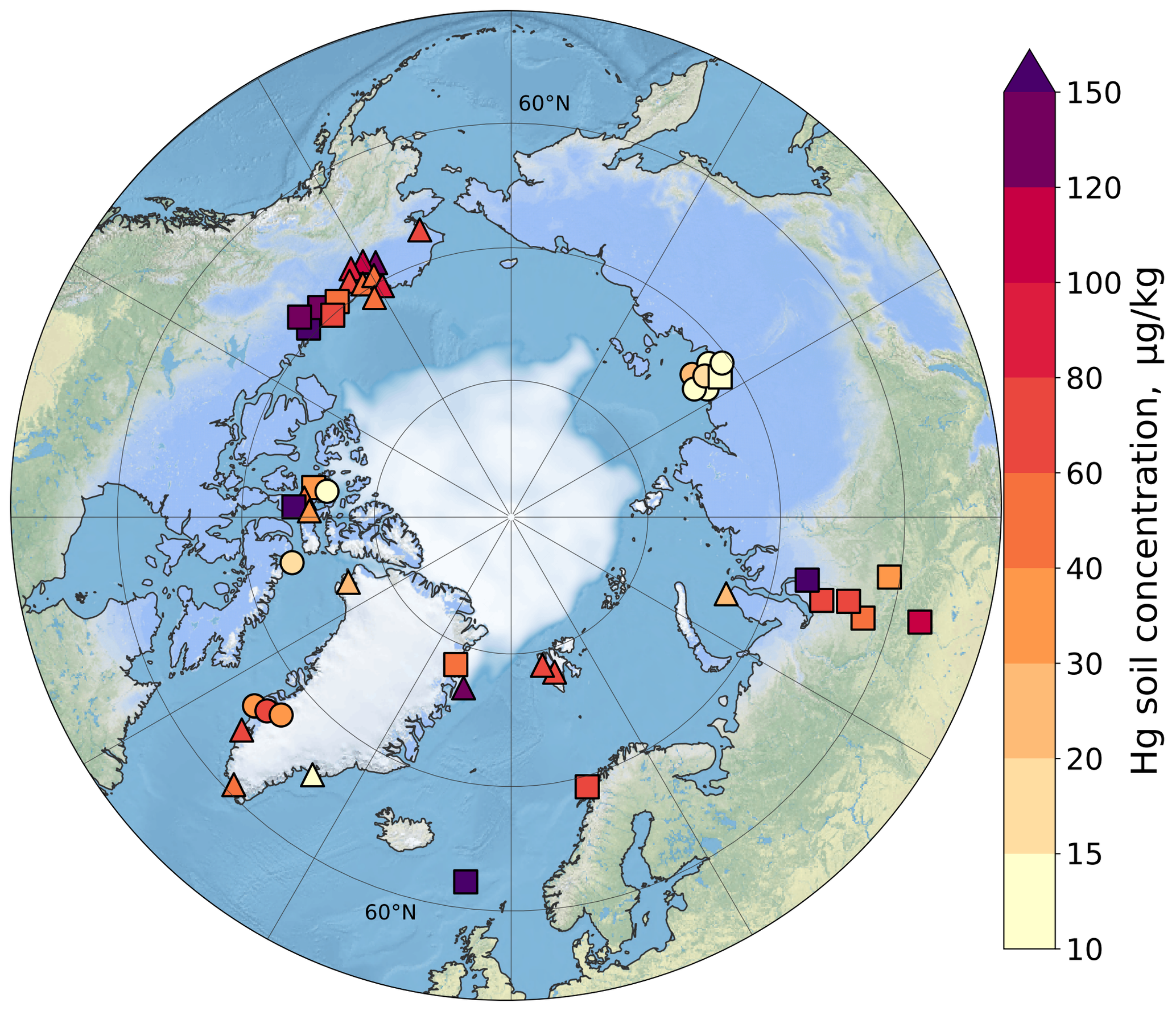
60°N
60°N
150
120
100
80
60
40
30
20
15
10
Hg soil concentration, µg/kg

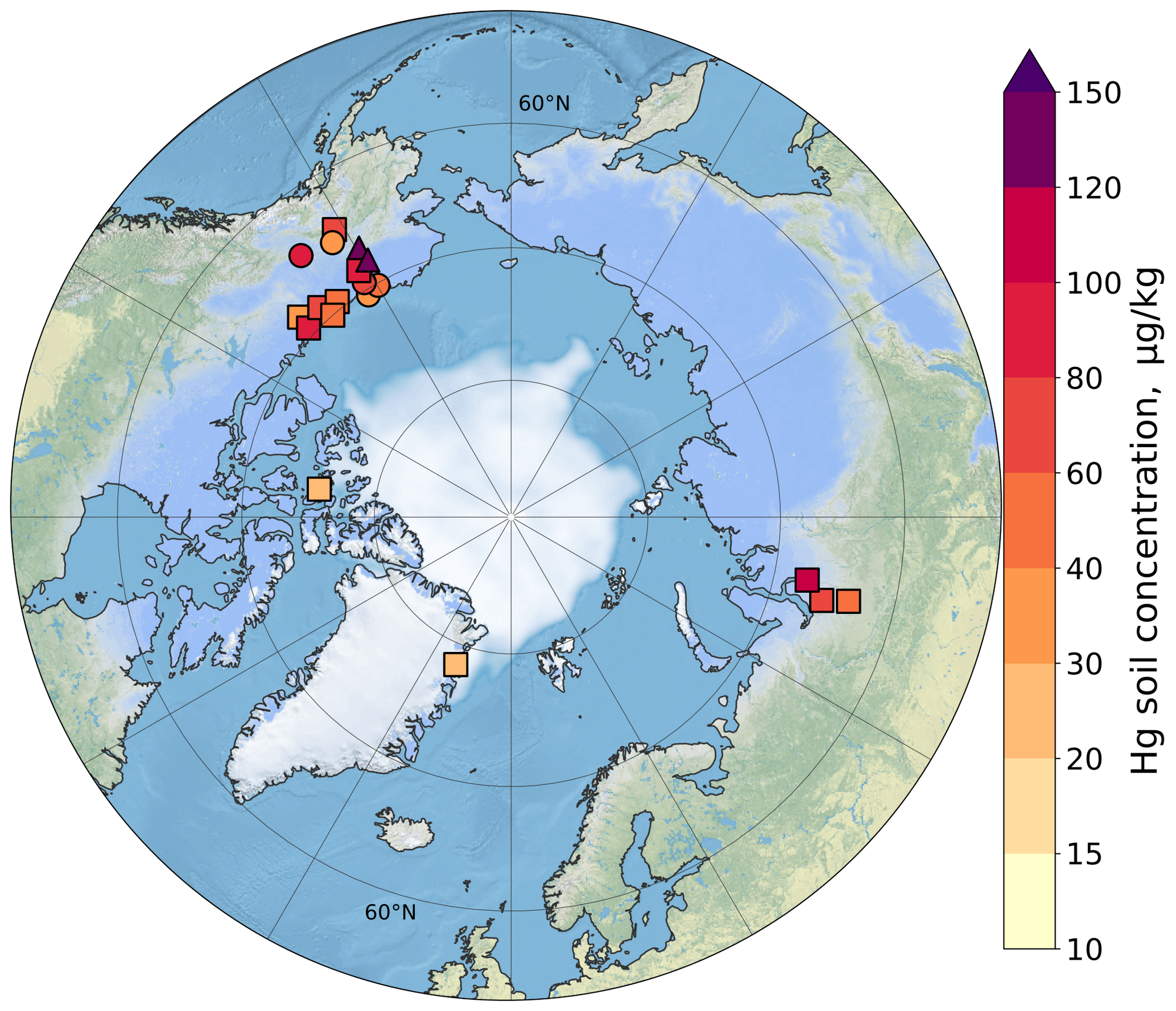
60°N
60°N
150
120
100
80
60
40
30
20
15
10
Hg soil concentration, µg/kg

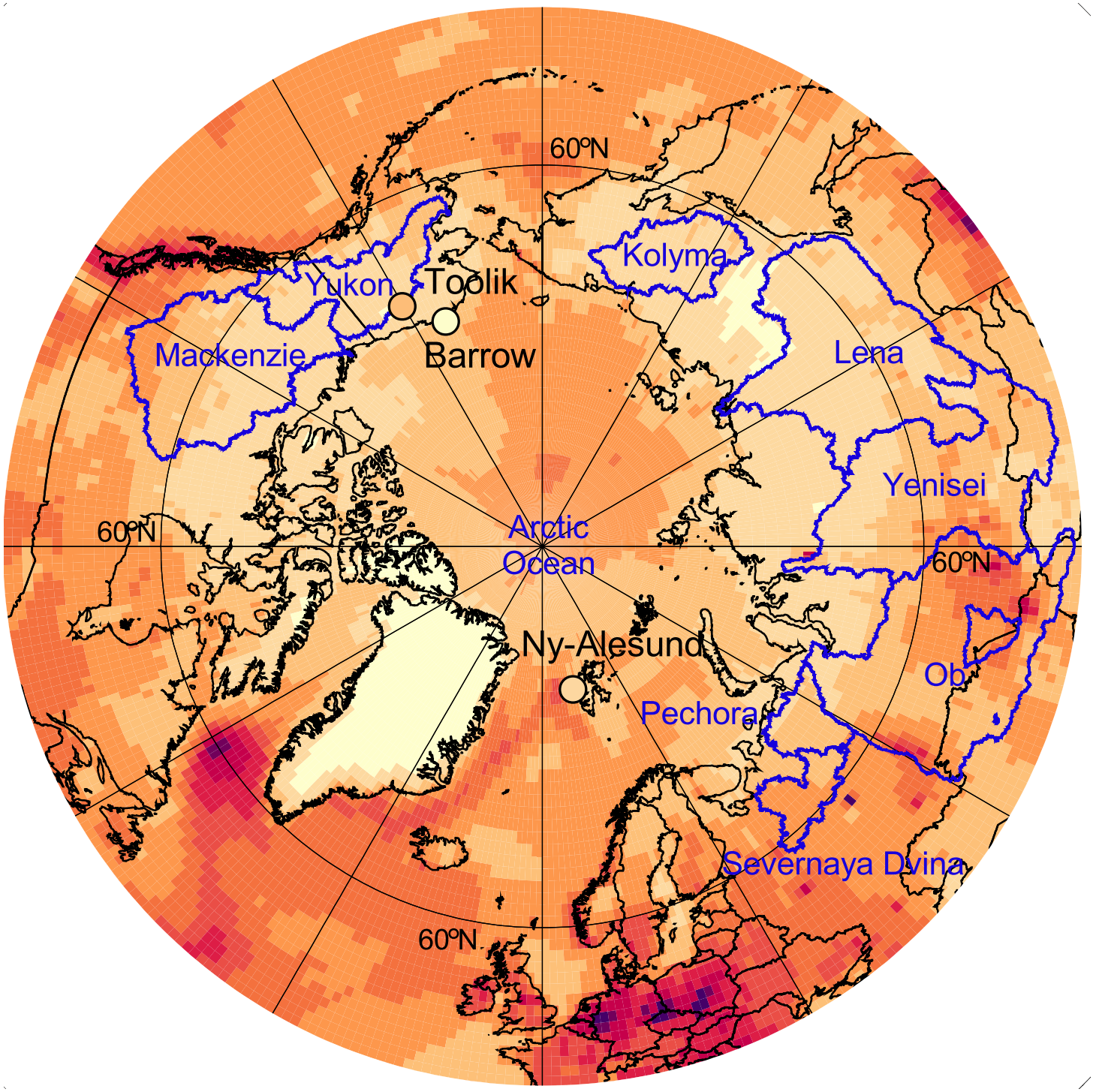
60°N
Kolyma
Yukon
Toolik
Barrow
Mackenzie
Lena
Yenisei
60°N
Arctic
Ocean
60°N
Ny-Alesund
Ob
Pechora
Severnaya Dvina
60°N

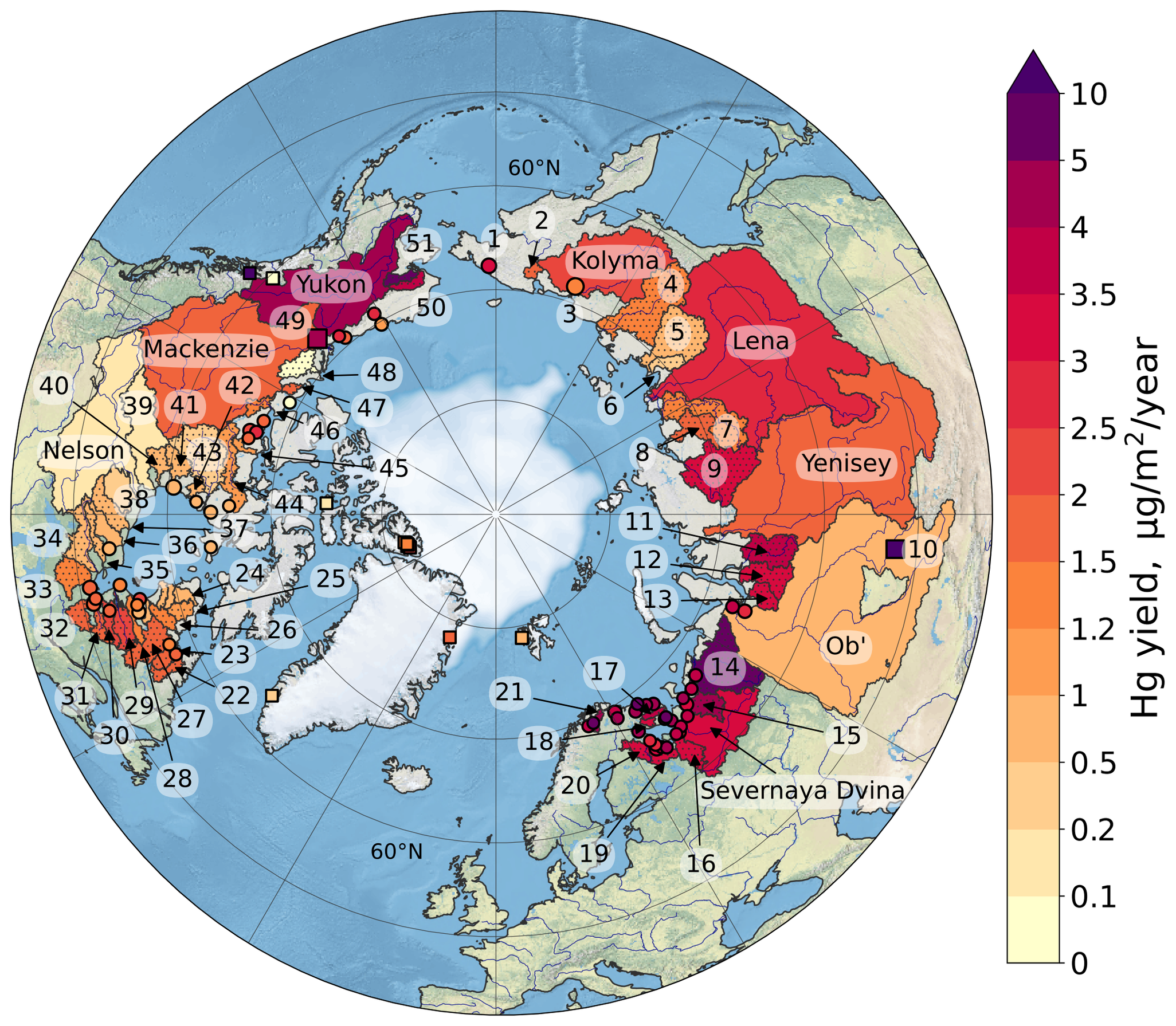
60°N
60°N
Yukon
Mackenzie
Nelson
Kolyma
Lena
Yenisey
Ob'
Severnaya Dvina
1
2
3
4
5
6
7
8
9
10
11
12
13
14
15
16
17
18
19
20
21
22
23
24
25
26
27
28
29
30
31
32
33
34
35
36
37
38
39
40
41
42
43
44
45
46
47
48
49
50
51
Hg yield, µg/m²/year
0
0.1
0.2
0.5
1
1.2
1.5
2
2.5
3
3.5
4
5
10

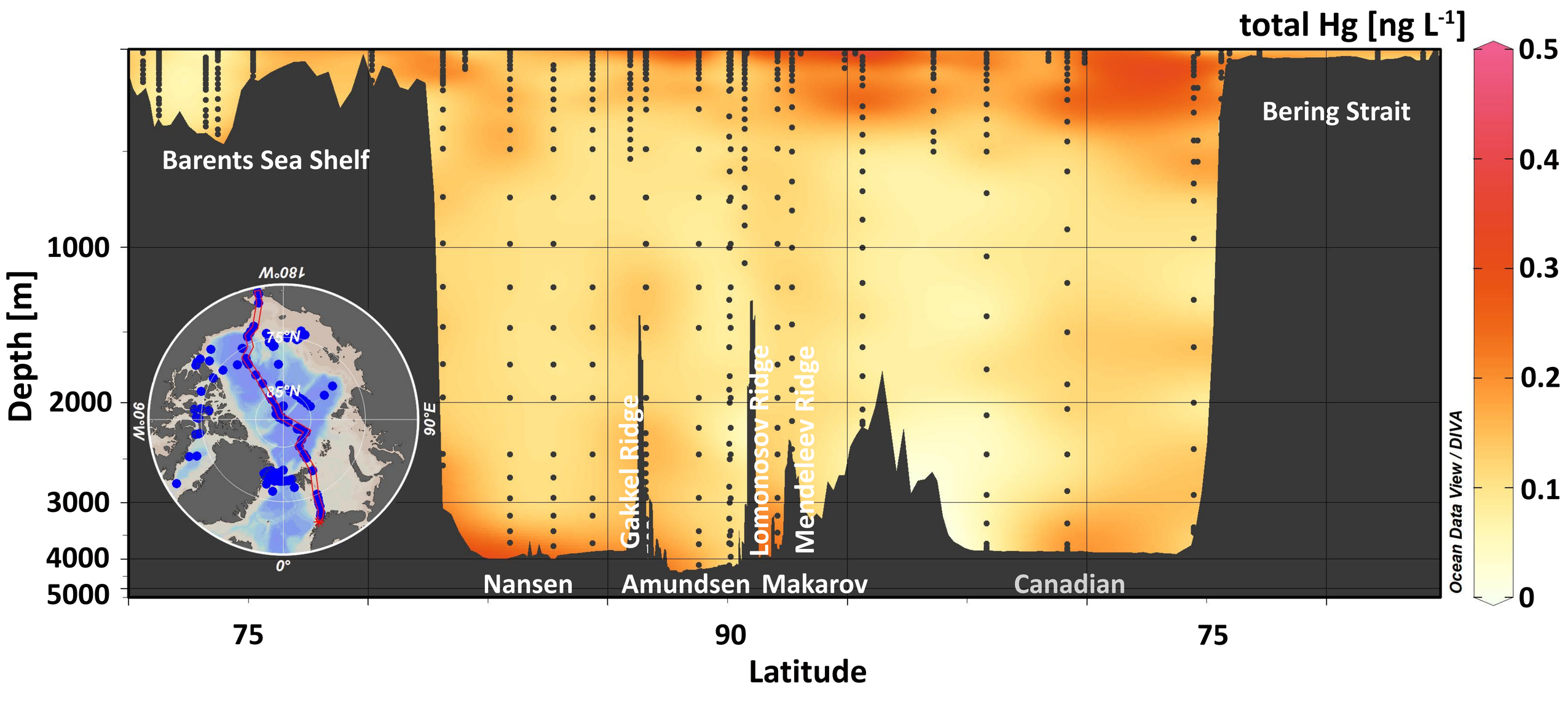
total Hg [ng L-1]
Barents Sea Shelf
Bering Strait
Depth [m]
1000
2000
3000
4000
5000
Nansen
Amundsen
Makarov
Canadian
Gakkel Ridge
Lomonosov Ridge
Mendeleev Ridge
75
90
75
Latitude
0.5
0.4
0.3
0.2
0.1
0
Ocean Data View / DIVA
180°W
90°W
0°
90°E
75°N
85°N

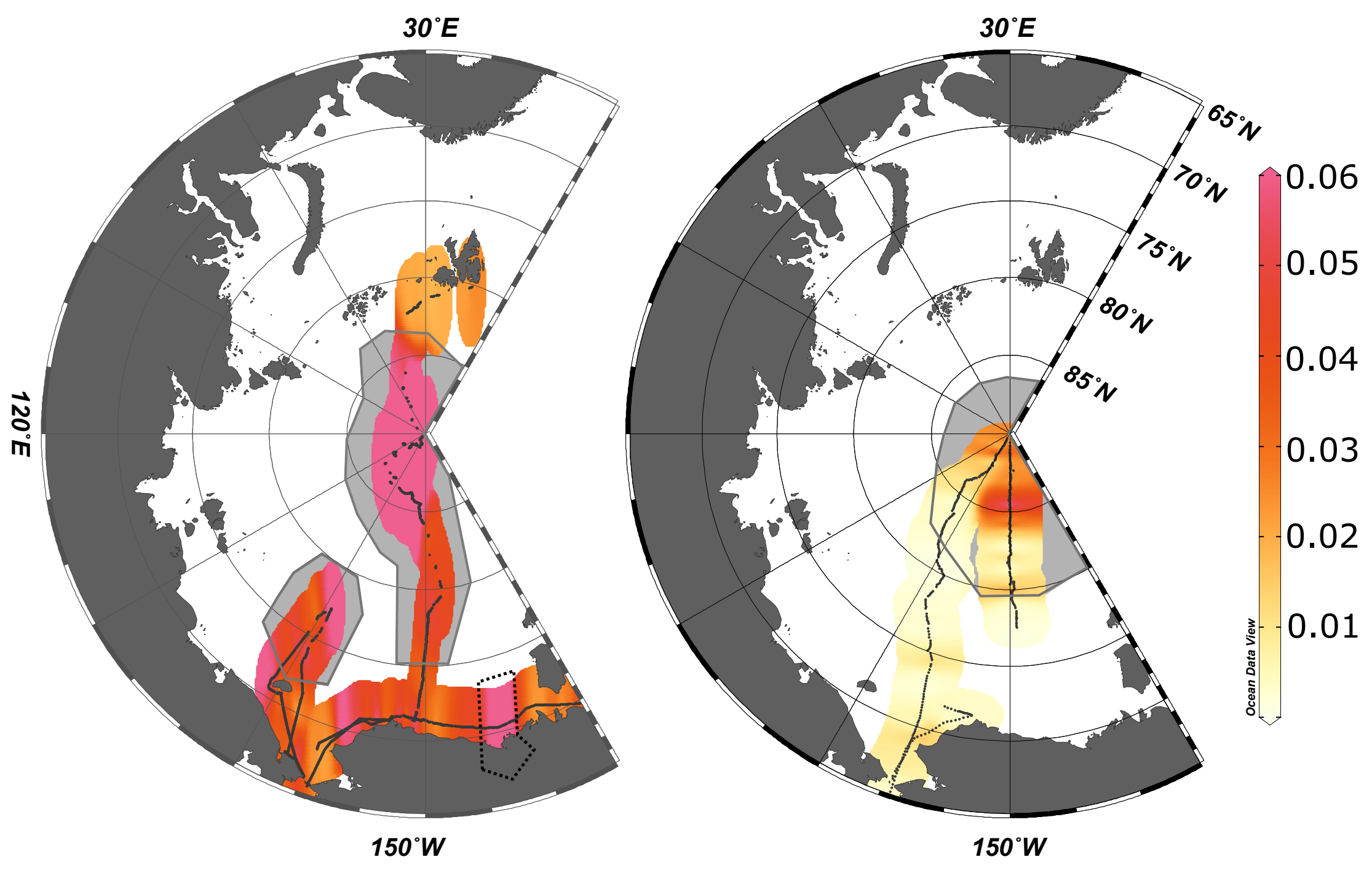
30˚E
120˚E
150˚W
30˚E
65˚N
70˚N
75˚N
80˚N
85˚N
150˚W
0.06
0.05
0.04
0.03
0.02
0.01
Ocean Data View

Atmosphere

330

Total Hg

Flux: Mg/y

Hg budget: Mg

a 14

b 24 soils/vegetation

c 9

e 118

Glaciers 2,415

Snowpacks 39

d 32

f 65

h 41

g 39

49,000 Surface soils (0-0.3m)

212,000 Active layer (0-1m)

597,000 Permafrost (0-3m)

o 122

9

1.4 k

44 0-20m

7 p

228 20-200m

q

m 42

5 j

l 73

224 200-500m

i 55

1,375 500-base

Arctic Ocean

r

s

4 n

Sediments
(Hg concentration: 29 ng/g)

Sediments
(Hg concentration: 60 ng/g)